J. Fluid Mech. (1992), *vol.* 237, *pp.* 569–603
Printed in Great Britain

The effects of curvature on sheared turbulence

By A. G. L. HOLLOWAY† AND S. TAVOULARIS
Department of Mechanical Engineering, University of Ottawa, Ottawa, Canada K1N 6N5

(Received 18 May 1990 and in revised form 9 August 1991)

The present experiments are an extension of previous studies on nearly homogeneous, parallel, shear flows and represent an attempt to study the effects of curvature on sheared turbulence in relative isolation from wall and entrainment effects. Uniformly sheared turbulence was allowed to reach a state of transverse statistical homogeneity in a straight rectangular duct; it was then passed into a curved duct, also of rectangular cross-section. The near homogeneity of the turbulence and the near uniformity of the shear were preserved. In the present experiments, the parameter $S = (U_c/R_c)/(\mathrm{d}U/\mathrm{d}n)$ spanned a wide range, from approximately -0.50 to over 1.0 (U_c is the centreline velocity, $\mathrm{d}U/\mathrm{d}n$ the mean shear and R_c the radius of curvature on the centreline of the duct). Variation of S was achieved by using two curved tunnel sections as well as by adjusting the shear. Measurements indicate that the growth of the turbulent stresses and lengthscales was enhanced for $S < 0$ and suppressed for $S > 0$. For $S > 0.05$, the stresses decayed. In cases where sufficiently large total strain was achieved, the stresses seemed to grow or decay roughly exponentially and to develop in a quasi-self-preserving manner. The magnitude of the dimensionless shear stress decreased monotonically with increasing S, while, for sufficiently large positive values of S, this quantity reversed sign, to achieve the same sense as the mean shear. Measurements of the integral lengthscales and the Taylor microscales are presented and their dependence upon curvature discussed. The results in 'mildly curved' flows are used to derive approximate expressions for the dependence upon S of the various terms in the Reynolds stress equations, including the pressure–strain rate covariance tensor.

1. General introduction and a review of the literature

The instantaneous streamlines of all turbulent motions are highly curved. With few exceptions, turbulent shear flows also display mean streamline curvature.

The importance of curvature effects varies widely from one shear flow to another. For example, the curvature of the mean streamlines in the boundary layer along a flat plate is so slight that its effects are essentially unnoticeable, while in some vortex flows the turbulence structure is dominated by curvature effects. Curvature can have a stabilizing or destabilizing effect on the fluid motion, depending on the direction of the curvature with respect to the flow velocity and its gradient, and it affects both the process of transition to turbulence and the evolution of fully turbulent motions. It has been well documented that even slight boundary curvature introduces significant changes in skin friction. Stronger boundary curvature is known to generate streamwise vorticity.

A better understanding of the interaction between streamline curvature and shear may provide insight into drag reduction and perhaps lead to a better design of

† Present address: Department of Mechanical Engineering, University of New Brunswick, Fredericton, Canada E3B 5A3.

vehicles and fluid machinery. Most analyses of curved shear flows have been concerned with the stability of basic motions, i.e. of 'simple' solutions of the governing equations. Rayleigh (1916) and Synge (1933) studied inviscid flow and found it unstable in cases where the angular momentum decreased with increasing radius. Taylor (1923) and Synge (1938) studied viscous flow between rotating cylinders and found that, for stability of small axisymmetric disturbances, the circulation of the outer cylinder must have the same sense as and be greater than that of the inner cylinder. Görtler (1940) examined the stability of curved boundary layers and Dean (1928) the stability of Poiseuille flow in curved circular pipes. These authors concluded that linear instability analysis can predict the formation of longitudinal vortices. Although the relevance of linear analyses to fully turbulent flows is, at best, questionable, such analyses provide the only available mathematical and physical basis for understanding curved turbulent flows.

A fair number of experimental studies of turbulent curved shear flows, mostly with two-dimensional curvature, have been published in recent years. Many of these can be classified as (*a*) boundary layers along convex and concave surfaces, (*b*) curved free shear flows, and (*c*) curved duct flows.

Measurements of the turbulence in convex boundary layers have been performed by So & Mellor (1973), Meroney & Bradshaw (1975), Smits, Young & Bradshaw (1979), Ramaprian & Shivaprasad (1978*a*, *b*, 1982), Gillis & Johnston (1983), Gibson, Verriopoulos & Vlachos (1984), Gibson & Verriopoulos (1984) and Muck, Hoffman & Bradshaw (1985). With the exception of the experiments by So & Mellor (1973), these are cases with relatively mild curvature.

Measurements of the turbulence in concave boundary layers have been performed by Meroney & Bradshaw (1975), So & Mellor (1975), Smits *et al.* (1979), Nakano *et al.* (1981), Ramaprian & Shivaprasad (1978*a*, *b*, 1982), Shizawa & Honami (1985), Hoffman, Muck & Bradshaw (1985) and Barlow & Johnston (1988*a*, *b*). So & Mellor (1975) used strong curvature and observed longitudinal vortices in the mean flow.

Among the above studies, it appears that the measurements of Ramaprian & Shivaprasad (1978*a*, *b*, 1982) describe most comprehensively the flow structure of curved boundary layers. The only experiments with some resemblance to the present study are those by Nakano *et al.* (1981), which considered the effect of free-stream turbulence, maintained by an approximately uniform shear, on a concave boundary layer. While the free-stream turbulence was not homogeneous, its intensity was found to increase when the velocity decreased away from the centre of curvature but not when the velocity increased away from the centre of curvature.

Turbulence measurements in curved free shear flows include those in strongly curved mixing layers by Margolis & Lumley (1965), Wyngaard *et al.* (1968) and Castro & Bradshaw (1976), and those in curved wakes by Savill (1983) and Koyama (1981). The measurements of Savill (1983) include multiple point velocity statistics.

Measurements of the turbulence in fully developed curved rectangular duct flow have been performed by Eskinazi & Yeh (1956) and Hunt & Joubert (1979). The direct numerical simulation of a relatively low-Reynolds-number, turbulent, curved, rectangular channel flow by Moser & Moin (1987) can also be used for comparison with experimental results.

The experimental results have consistently demonstrated an enhancement of turbulent mixing in cases where the velocity decreases away from the centre of curvature and a suppression of turbulent mixing where the velocity decreases towards the centre of curvature. These observations are compatible with the results of linear inviscid theory.

The above review demonstrates that significant efforts have been made to document the effects of curvature on bounded and free shear flows. Although most of these studies have been performed in relatively 'simple' laboratory configurations, they are invariably subject to the simultaneous action of several interacting mechanisms, such as the entrainment of irrotational flow, the proximity of viscous wall layers and the inevitable non-uniformity of the mean shear. The objective of the present research is to reduce and, if possible, to eliminate the interference of such mechanisms, so that the evolution of turbulence under the influence of 'pure' curvature and 'pure' shear can be revealed. To achieve this, the concept of non-stationary homogeneous turbulent shear flow (for a discussion see Hinze 1975) and its experimental approximation, the uniformly sheared turbulent flow (Champagne, Harris & Corrsin 1970), have been extended to include the effects of curvature. This extension is limited to cases where the turbulent lengthscales are small in comparison to the radius of curvature.

Although a very large volume of data was collected for this work, economy of presentation dictates that only the most significant, or, in some cases, representative results be presented here. More details can be found in the thesis of Holloway (1989).

2. Analytical description of homogeneous, non-stationary, curved shear flow

2.1. *Introduction*

In a curved shear flow the energy provided to the turbulence comes from the mean straining of the fluid as in rectilinear shear flows. The local strain is a function of the curvature. In addition, the flow curvature changes the turbulence structure, which, in turn, affects the efficiency of the energy transfer from the mean flow to the turbulence.

An ideal flow for studying the interaction of shear and curvature would be one where turbulence, curvature and shear are homogeneous. Such a flow can be conceived by extending the notion of rectilinear, homogeneous, shear flow to a flow with mean streamlines which are not parallel but form concentric rings. The shear should be assumed uniform in the radial direction but a fluid particle would on the average move along a curved path. It is easy to see that inhomogeneity of the turbulence would inevitably develop under such conditions, as a result of the transverse non-uniformity of the curvature and strain. Nevertheless, it seems worth exploring the plausibility of an approximately homogeneous curved shear flow by introducing additional constraints.

Consider a flow field bounded by two coaxial circular cylinders with a difference in radius that is large in comparison with the scales of the turbulence but small compared with the mean radius. Then the mean streamline curvature can be considered as nearly constant within the volume and the turbulence structure in the core of the volume can be assumed independent of wall effects, at least over a sufficiently small time interval. If the turbulence within this volume is homogeneous initially, it is likely to remain homogeneous for some time.

2.2. *Equations for the Reynolds stresses*

The flow introduced in the previous section can best be described in a curvilinear, orthogonal system of coordinates, similar to those commonly used in studies of curved boundary layers. These will be denoted by s, n and z, as shown in figure 1. The

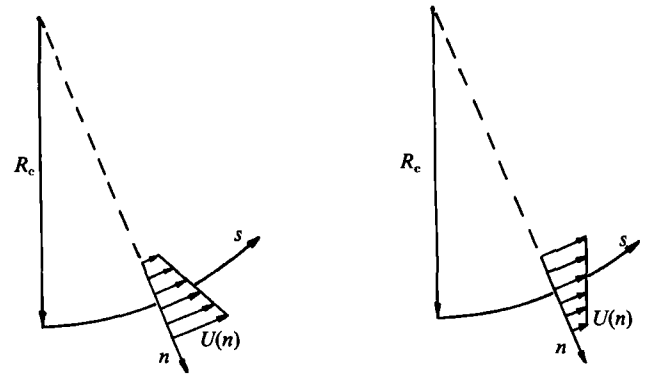

$S > 0$ $S < 0$

FIGURE 1. Schematic representation of simple curved shear flows.

s-coordinate is the length of a circular arc, with a radius R_c, coincident with the flow volume centreline. The n-coordinate is normal to s, has its origin on the volume centreline and is positive when directed away from the centre of curvature. The radial extent of the flow volume is assumed to be small compared to R_c. The z-coordinate is normal to both s and n and has a direction following the right-hand rule.

The local, instantaneous, velocity vector can be decomposed into means, U, V, W, and fluctuations, u, v, w, parallel, respectively, to the s, n, z directions. In flows with uniform mean shear in the n-direction alone, the mean velocity vector can be represented as

$$(U, V, W) = \left(U_c + \frac{\mathrm{d}U}{\mathrm{d}n} n, 0, 0\right), \tag{1}$$

where U_c is the centreline velocity, also assumed constant.

Non-dimensionalizing the coordinates and the turbulent quantities by using an appropriate lengthscale, l, an appropriate velocity scale, v, and the resulting timescale, $\mathscr{T} = l/v$, and with the additional assumptions of homogeneity of the turbulence, uniformity of the scales l, v and $\mathscr{T}$, two-dimensionality of the mean field and negligibility of the scale of turbulent motions compared to the radius of curvature ($l \ll R_c$), one may simplify (Holloway 1989) the equations describing the temporal evolution of the turbulent kinetic energy per unit mass and the non-vanishing Reynolds stresses into the following dimensionless forms

$$\kappa_q \frac{\overline{q^{*2}}}{2} + \frac{\partial}{\partial \tau}\frac{\overline{q^{*2}}}{2} = -\overline{u^* v^*}(1-S)\frac{\mathrm{d}U}{\mathrm{d}n}\mathscr{T} - \epsilon^*, \tag{2}$$

$$\kappa_q \overline{u^{*2}} + \frac{\partial}{\partial \tau}\overline{u^{*2}} = -2\overline{u^* v^*}(1+S)\frac{\mathrm{d}U}{\mathrm{d}n}\mathscr{T} + \phi^*_{uu} - 2\epsilon^*_{uu}, \tag{3}$$

$$\kappa_q \overline{v^{*2}} + \frac{\partial}{\partial \tau}\overline{v^{*2}} = 4\overline{u^* v^*} S \frac{\mathrm{d}U}{\mathrm{d}n}\mathscr{T} + \phi^*_{vv} - 2\epsilon^*_{vv}, \tag{4}$$

$$\kappa_q \overline{w^{*2}} + \frac{\partial}{\partial \tau}\overline{w^{*2}} = \phi^*_{ww} - 2\epsilon^*_{ww}, \tag{5}$$

$$\kappa_q \overline{u^* v^*} + \frac{\partial}{\partial \tau}\overline{u^* v^*} = (-\overline{v^{*2}}(1+S) + 2\overline{u^{*2}}S)\frac{\mathrm{d}U}{\mathrm{d}n}\mathscr{T} + \phi^*_{uv} - 2\epsilon^*_{uv}. \tag{6}$$

In the above equations, overbars denote ensemble averages and asterisks denote dimensionless quantities. The coefficient κ_q is defined as

$$\kappa_q = \frac{1}{v^2}\frac{\mathrm{d}(v^2)}{\mathrm{d}\tau} \tag{7}$$

and τ represents dimensionless time. The symbol ϵ^* represents the dimensionless dissipation rate of the turbulent kinetic energy and ϵ^*_{uu} etc. its components corresponding to the different turbulent stresses. The symbols ϕ^*_{uu} etc. represent the dimensionless pressure–strain rate covariances, defined, for example, as

$$\phi^*_{uu} = 2\overline{p^*\frac{\partial u^*}{\partial s^*}}. \tag{8}$$

Finally, the parameter S is defined as

$$S = \frac{U_c/R_c}{\mathrm{d}U/\mathrm{d}n}. \tag{9}$$

Clearly, S represents a relative measure of the curvature magnitude with respect to the mean shear. In an unsheared curved flow, $S \to \pm\infty$; in a non-curved shear flow, $S = 0$; in rigid body rotation, $S = 1$; and in irrotational flow, $S = -1$.

The above equations show that the curvature appears explicitly in 'production' terms in the equations for the streamwise and transverse components of kinetic energy and for the shear stress. In contrast, in a rectilinear shear flow, direct energy production appears only in the equations for the streamwise component of the turbulent kinetic energy and for the shear stress (Champagne *et al.* 1970).

Note that, if the scales v and $\mathscr{T}$ are chosen such that the parameters κ_q and $|\mathrm{d}U/\mathrm{d}n|\mathscr{T}$ are constant, then the dimensionless statistics, namely the solutions of (2)–(6), would become functions of τ and S only. Equation (7) shows that constancy of κ_q implies an exponential variation of v (note that constancy of v would be regarded as a degenerate exponential change).

2.3. *Scales for the evolution of turbulence*

In a rectilinear homogeneous shear flow, if one chooses the characteristic timescale, $\mathscr{T}$, to be equal to the inverse mean shear, $|\mathrm{d}U/\mathrm{d}n|^{-1}$, the dimensionless time, τ, becomes equal to the total mean strain of a fluid element and, hence, proportional to the energy transferred from the mean flow to the turbulence (Harris, Graham & Corrsin 1977). In a curved homogeneous shear flow the mean strain rate is $\frac{1}{2}(1-S)\,\mathrm{d}U/\mathrm{d}n$ and the total mean strain during the time t is $t(1-S)\,\mathrm{d}U/\mathrm{d}n$. Therefore, it seems logical to maintain $|\mathrm{d}U/\mathrm{d}n|^{-1}$ as the characteristic time in curved flows, at least those with $|S| \ll 1$. It could also be pointed out that, in the limiting case when $S = 1$ (rigid body rotation), there is no mean straining of the fluid; however, $|\mathrm{d}U/\mathrm{d}n|^{-1}$ would also be a characteristic time, being proportional to the period of flow turning. With this choice of timescale, (2)–(6) can be further simplified, by substituting

$$(\mathrm{d}U/\mathrm{d}n)\,\mathscr{T} = \operatorname{sgn} S, \tag{10}$$

where $\operatorname{sgn} S = 1$, if $S > 0$, and -1, if $S < 0$.

In an unbounded, rectilinear, homogeneous shear flow there is no lengthscale associated with the mean field. Furthermore, because a coordinate transformation to a frame convected with the mean speed should be Galilean (Harris *et al.* 1977), the mean velocity cannot be used as a velocity scale. Therefore, a velocity scale (or

lengthscale) must be defined from consideration of the turbulence field. A convenient choice for the velocity scale, v, would be the r.m.s. speed of the turbulent fluctuations, q'. When combined with the timescale, this yields the lengthscale

$$l = q'/|\mathrm{d}U/\mathrm{d}n|. \tag{11}$$

In a curved homogeneous shear flow the radius of curvature of the mean flow, R_c, represents an apparent external lengthscale. Furthermore, unlike in the straight flow case, a frame fixed with the curved mean flow is not inertial and the mean convection speed, U_c, cannot be excluded as a velocity scale. In the present type of flow, R_c is very large in comparison with the scales of the turbulence and it is unlikely that turbulent motions would scale with it. Besides, a perfectly homogeneous flow should be independent of any external lengthscale. The dependence of flow structure upon U_c and R_c can, however, be accommodated, if one notices that the ratio R_c/U_c provides another timescale for the flow, in addition to $|\mathrm{d}U/\mathrm{d}n|^{-1}$. The equations for the Reynolds stresses lend some support to this hypothesis, because, in the limit of $l/R_c \to 0$, all isolated appearances of R_c vanish, while the appearance of the ratio R_c/U_c persists. This ratio represents a period of turning of the flow, as can be seen by analogy to the case of rigid body rotation, where R_c/U_c is precisely the period of rotation and τ is equal to the angle of rotation. In view of this discussion, S can be interpreted as the ratio of timescales characteristic of mean shear and rotation effects. When S is small, shear effects should dominate, as they are imposed at a faster pace on the turbulence structure. When S is large, turbulence production should be dominated by curvature effects and the appropriate timescale should be R_c/U_c. At intermediate values of S, turbulence production is substantially affected by both shear and curvature and the timescale characterizing the turbulence structure would likely be one intermediate between $|\mathrm{d}U/\mathrm{d}n|^{-1}$ and R_c/U_c; the average of these two scales is clearly an inappropriate choice because it leads to incorrect limits as $S \to 0$ or $\pm\infty$; the harmonic average overcomes this problem and would, perhaps, be more appropriate, although one should anticipate that coupling of the two production mechanisms would make a simple relationship between timescales unlikely. In any case, R_c and U_c should not be used as independent length and velocity scales associated with the mean flow and such scales must be defined from the turbulence field. As in the straight shear flow, one may choose q' and l (equation (11)) as the most appropriate scales.

Based on the above discussion, it seems plausible that all dimensionless turbulence statistics in a curved homogeneous shear flow would depend only on the dimensionless time, τ, and the ratio, S, of the timescales of the mean field. Further relaxation of dependence on τ would be equivalent to a hypothesis of self-preservation of the turbulence structure, a possibility discussed in the next section.

2.4. *Consequences of self-preservation*

Tavoularis (1985) has introduced the hypothesis that rectilinear, uniformly sheared, transversely homogeneous turbulence would evolve asymptotically to a self-preserving state for which the dimensionless statistics would be independent of τ and where the velocity and length scales would grow or decay exponentially. These arguments can easily be extended to homogeneous, curved shear flow. Substituting $v = q'$ in (2) and defining the dimensionless shear stress as $K_{uv} = \overline{uv}/\overline{q^2}$ $(= \overline{u^*v^*})$, one gets

$$\frac{1}{\overline{q^2}}\frac{\partial \overline{q^2}}{\partial \tau} = 2P^* - 2\epsilon^*, \tag{12}$$

where the dimensionless 'production', P^*, and 'dissipation', ϵ^*, are, respectively, defined as

$$P^* = -K_{uv}(1-S)\,\mathrm{sgn}\,S \tag{13}$$

and

$$\epsilon^* = \frac{\epsilon}{\overline{q^2}|\mathrm{d}U/\mathrm{d}n|}. \tag{14}$$

As in the rectilinear shear flow case, if K_{uv}, S and ϵ^* are assumed to be independent of τ, then $\overline{q^2}$ must be an exponential function of τ, namely,

$$\overline{q^2} = \overline{q_0^2}\,\mathrm{e}^{\kappa_q(\tau-\tau_0)}, \tag{15}$$

where $\overline{q_0^2}$ is the value of $\overline{q^2}$ at a reference time τ_0. Similarly, if one further assumes that all dimensionless Reynolds stresses, K_{uu}, K_{vv}, K_{ww} and K_{uv}, have constant asymptotic values, then it follows that all Reynolds stresses would change exponentially, at the same rate as the kinetic energy.

2.5. *The pressure–strain rate covariance tensor*

The pressure–strain rate covariances, which appear in the Reynolds stress equations, are believed to play an important role in the redistribution of turbulent kinetic energy into its three components and in the development of the shear stress. Pressure–strain rate covariances are too difficult to measure accurately, but, as demonstrated by Champagne *et al.* (1970), Harris *et al.* (1977) and Tavoularis & Karnik (1989, hereinafter referred to as TK), they can be estimated from the Reynolds stress equations as the balance of the other terms. We shall attempt to extend TK's simplified estimates of these quantities to self-preserving, curved, uniformly sheared flows.

The total dissipation rate, ϵ^*, can be estimated as the balance of the other, measurable terms in (12). For estimating the partition of the dissipation rate into its components, it seems worth exploring two plausible hypotheses, namely that (*a*) the dissipation is isotropic, and (*b*) the dissipation is anisotropic but its anisotropy is equal to the anisotropy of the Reynolds stresses. The first hypothesis was used, among others, by Champagne *et al.* (1970) and is based on the assumption that dissipation depends primarily on motions corresponding to high wavenumbers, which would become isotropic at large Reynolds numbers (for a thorough discussion see Hinze 1975). The second hypothesis was introduced by TK and assumes that the anisotropy, imposed by the mean strain and most noticeable at the low wavenumbers, persists even at the higher wavenumbers, which are responsible for the dissipation. The actual anisotropy of the dissipation tensor could be bounded by the two cases presented above; for this reason we shall pursue the implications of both hypotheses.

For an isotropic dissipation, (3)–(6) lead to the expressions

$$\phi^*_{uu} = (K_{uu}-\tfrac{1}{3})\,\kappa_q + \tfrac{4}{3}K_{uv}(1+2S)\,\mathrm{sgn}\,S, \tag{16}$$

$$\phi^*_{vv} = (K_{vv}-\tfrac{1}{3})\,\kappa_q - \tfrac{2}{3}K_{uv}(1+5S)\,\mathrm{sgn}\,S, \tag{17}$$

$$\phi^*_{ww} = (K_{ww}-\tfrac{1}{3})\,\kappa_q - \tfrac{2}{3}K_{uv}(1-S)\,\mathrm{sgn}\,S, \tag{18}$$

$$\phi^*_{uv} = K_{uv}\,\kappa_q + [K_{vv}(1+S) - 2K_{uu}S]\,\mathrm{sgn}\,S. \tag{19}$$

For a dissipation having the same anisotropy as the Reynolds stresses, (3)–(6) lead to the expressions

$$\phi^*_{uu} = 2K_{uv}[(1-K_{uu}) + (1+K_{uu})\,S]\,\mathrm{sgn}\,S, \tag{20}$$

$$\phi^*_{vv} = -2K_{uv}[K_{vv} + (2-K_{vv})\,S]\,\mathrm{sgn}\,S, \tag{21}$$

$$\phi^*_{ww} = -2K_{uv}K_{ww}(1-S)\,\mathrm{sgn}\,S, \tag{22}$$

$$\phi^*_{uv} = [(K_{vv}-2K_{uv}^2) + (K_{vv}-2K_{uu}+2K_{uv}^2)\,S]\,\mathrm{sgn}\,S. \tag{23}$$

One may note that (20)–(23) are independent of κ_q. It is also interesting to note that, when the dimensionless pressure–strain rate covariances are normalized by the dimensionless 'production' of turbulent kinetic energy, (20)–(22) take the following, simpler forms:

$$\frac{\phi^*_{uu}}{P^*} = 2K_{uu} - 2\frac{1+S}{1-S}, \tag{24}$$

$$\frac{\phi^*_{vv}}{P^*} = 2K_{vv} + 4\frac{S}{1-S}, \tag{25}$$

$$\frac{\phi^*_{ww}}{P^*} = 2K_{ww}. \tag{26}$$

3. Qualitative predictions of curvature effects

At this point, it seems useful to attempt to generate some insight into the mechanisms by which curvature affects turbulence by pursuing some elementary physical and analytical considerations.

Momentum conservation dictates that turning of the mean flow along a curved streamline must be accompanied by a transverse mean pressure gradient, which is proportional to the mean centripetal acceleration. In a turbulent flow, a particle with velocity higher than the mean ($u > 0$) and, thus, with higher inertia, would tend to resist this turning more than the average, with the result that it would tend to develop a motion away from the centre of curvature and, therefore, a positive transverse velocity fluctuation ($v > 0$). Similarly, a particle with $u < 0$ would tend to develop $v < 0$. In conclusion, curvature would tend to create a positive correlation uv. When $S < 0$, curvature would enhance the production of shear stress by the mean shear, while when $S > 0$, curvature would oppose this production.

The same conclusion, concerning production of shear stress, can be reached by observation of the production terms in (6), rewritten in dimensional rather than dimensionless form. In a rectilinear flow, the production term would be $-\overline{v^2}(\mathrm{d}U/\mathrm{d}n)\mathscr{T}$, which has the same sign as $\overline{uv}$ and would tend to increase the magnitude of $\overline{uv}$, independently of its sign. In a curved flow, the additional 'production', $(2\overline{u^2}-\overline{v^2})S(\mathrm{d}U/\mathrm{d}n)\mathscr{T}$, would generally be positive and would tend to produce a positive shear stress. As a result, curvature would enhance mean shear production when $S < 0$, and oppose it when $S > 0$.

The effects of curvature on the production of turbulent stresses are expressed in two ways: explicitly, through the appearance of terms proportional to S, and implicitly, through the resulting changes of the turbulence structure (e.g. the value of $\overline{u^*v^*}$), which, in turn, enhance or suppress production by the mean shear. Focusing on the explicit production terms in (2)–(5), rewritten in dimensional form, it is easy to see that curvature tends to produce additional $\overline{v^2}$ and $\overline{q^2}$ when $S < 0$, and to suppress the production of these quantities when $S > 0$. It is curious to note that curvature tends to have the opposite effect on the explicit 'production' term for $\overline{u^2}$, namely it enhances production when $S > 0$, and suppresses it when $S < 0$. Because, however, the explicit production of $\overline{v^2}$ by curvature is twice as large as the corresponding, opposite production of $\overline{u^2}$, the net production of $\overline{q^2}$ agrees in sense with that of $\overline{v^2}$. There is no explicit production of $\overline{w^2}$ by either the mean shear or the curvature.

In view of the above discussion, exposing the diverse, explicit effects of curvature upon the production of turbulent stresses, and the expectation (supported by measurements) that the dimensionless stresses would approach constant values, one must conclude that the pressure–strain rate correlation terms must play a very active role in the energy redistribution in curved shear flows. The strong coupling of pressure and velocity fluctuations could be related to the coupling of the mean velocity and pressure fields, due to streamline curvature.

The above discussion also leads to a classification of curved shear flows, depending upon whether curvature tends to enhance or oppose the production of turbulent shear stress and kinetic energy by the mean shear. In flows with $S < 0$, curvature effects would, generally, be 'destabilizing', i.e. tending to enhance the growth of turbulent activity, while, in flow with $S > 0$, curvature effects would be 'stabilizing', i.e. tending to suppress the growth of turbulent activity. In the latter case, whether turbulence grows or diminishes would depend on the relative magnitudes of shear and curvature. One may anticipate that for small, positive S turbulence might continue to grow but at a reduced rate compared to that in a corresponding rectilinear flow, whereas for large, positive S the turbulence might decay. Because curvature tends to produce positive shear stress, the possibility also arises that, for sufficiently large, positive S, uv might attain the same sign as the mean shear, contrary to the gradient transport concept.

The previous discussion applies to flows with significant shearing rates (e.g. $|S| < 1$). It would also be of interest to consider the limiting case of very weak shear ($S \to \pm\infty$). Here, the direction of shear and, therefore, the sign of S, should be inconsequential because turbulence production should be dominated by curvature effects. The forms of (2) and (6) in this limiting case confirm this expectation and they also point to an anisotropic asymptotic turbulence structure with a positive shear stress.

4. Stationary, transversely homogeneous, uniformly sheared, curved flow

Homogeneous turbulence is difficult to generate and maintain experimentally. Laboratory approximations to homogeneous flow are usually stationary in the laboratory frame but inhomogeneous in the streamwise direction. A laboratory flow of this type studied in the convected frame may have a close relation to a homogeneous flow, provided that the streamwise inhomogeneity is small (Corrsin 1963). Examples include grid-generated turbulence as an approximation to isotropic turbulence and uniformly sheared turbulence as an approximation to homogeneous shear flow.

As an approximation to the homogeneous curved shear flow, presented in section 2, we will extend the study of rectilinear, uniformly sheared turbulence by including curvature effects. Detailed derivations and forms of the governing equations have been reported by Holloway (1989). We shall assume that the flow is stationary, two-dimensional on the mean and that the mean streamlines are concentric circular arcs, as shown in figure 1. Continuity of the mean flow requires that, if $V = W = 0$, then U cannot be a function of s. Conservation of energy also requires that, if the kinetic energy of turbulence changes downstream, it must be balanced by an opposite change of the mean static pressure. An alternative possibility (Hinze 1975) is that the static pressure could be independent of s, while the change of turbulence kinetic energy would be balanced by a streamwise change of the mean kinetic energy; in such a case, continuity requires that $V \neq 0$. Any combination of these two

mechanisms is also possible but, if the change of the kinetic energy of the turbulence is relatively small, then any change in pressure or U may be neglected. Finally, conservation of transverse mean momentum, combined with transverse homogeneity, requires that a transverse gradient of mean pressure be created as a result of streamline curvature.

The equations describing the balance of the Reynolds stresses and the turbulent kinetic energy can be simplified into forms which resemble but are distinct from (2)–(6): as an example, we present the turbulent kinetic energy equation, which becomes

$$\aleph\left(U_c+\frac{\mathrm{d}U}{\mathrm{d}n}n\right)\frac{\partial}{\partial s}\frac{\overline{q^2}}{2}=-\overline{uv}\frac{\mathrm{d}U}{\mathrm{d}n}+\frac{\aleph}{R_c}\overline{uv}\left(U_c+\frac{\mathrm{d}U}{\mathrm{d}n}n\right)$$
$$-\left[\aleph\frac{\partial}{\partial s}\left(\frac{\overline{pu}}{\rho}+\frac{\overline{uq^2}}{2}\right)+\aleph\frac{\partial}{\partial n}\left(\frac{\overline{pv}}{\rho\aleph}+\frac{\overline{vq^2}}{2\aleph}\right)\right]+\text{viscous terms}, \quad (27)$$

where
$$\aleph=\left(1+\frac{n}{R_c}\right)^{-1}. \quad (28)$$

As in the case of rectilinear shear flows, exact transverse homogeneity of the turbulence would be incompatible with a variation of U in the n-direction, because terms corresponding to convection of a property by the mean flow would vary transversely. The equations would become self-consistent only if the turbulence were streamwise homogeneous and the curvature effects were negligible, but this would also require that the production and dissipation of the turbulence would exactly balance, which is a singular condition that is not generally met. This problem has already been identified for rectilinear, uniformly sheared flow by Champagne *et al.* (1970), who concluded that, if the flow were inhomogeneous in the streamwise direction, then it would also have to be transversely inhomogeneous.

A uniformly sheared, developing, laboratory flow would be rendered equivalent to a non-stationary homogeneous, curved shear flow by the transformation

$$U\frac{\partial(\,)}{\partial s}=\frac{\partial(\,)}{\partial t}, \quad (29)$$

i.e. by describing the flow structure in a frame convected with the mean speed. If one further assumes small inhomogeneity and large radius of curvature, compared to the transverse flow extent, the equations describing Reynolds stress development become identical in the two cases.

5. Experimental apparatus and measuring procedures

5.1. *The wind tunnel and the curved sections*

The wind tunnel at the University of Ottawa (figure 2) has been described in detail by Karnik & Tavoularis (1987, hereinafter referred to as KT). Following a 16:1 contraction, the flow passed through the shear generator comprising 12 separate parallel channels each with a height $M = 25.4$ mm, the flow separator which tended to make the larger scales of the flow uniform, and a straight rectangular section at height $h_s = 305$ mm, width 457 mm and length 3193 mm, before entering the curved section.

The straight section was equipped with four frames, permitting the insertion of

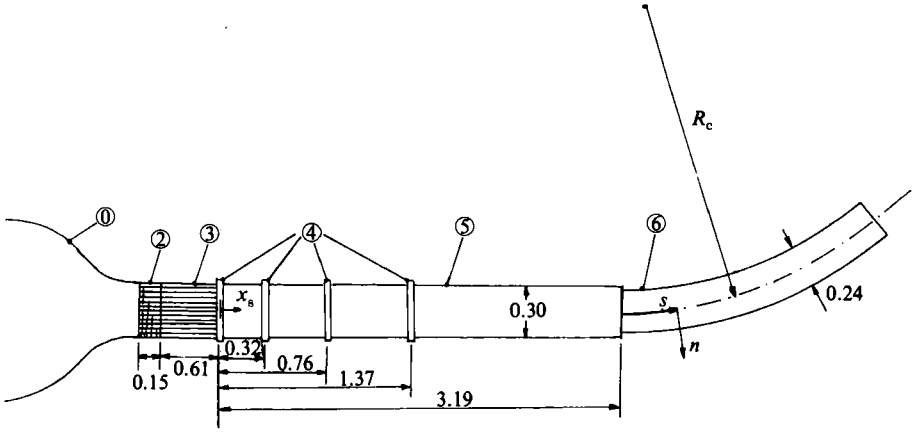

FIGURE 2. Sketch of the wind tunnel, showing the 16:1 contraction (1), the shear generator (2), the flow separator, (3), the four slots for the insertion of grids and screens (4), the straight test section (5) and a curved test section (6); all dimensions are in m.

grids and screens across the flow. As KT have shown, uniform obstructions reduce the magnitude of shear, while preserving the linearity of the mean velocity. For the present experiments, the downstream half of the straight test section that was used by KT and TK was removed and replaced by either of two interchangeable curved sections. The curved sections were designed to introduce two distinct degrees of curvature: a mild curvature, which would, presumably, introduce a small perturbation to the straight shear flow structure; and a strong curvature, which would create more pronounced effects.

Boundary layers are considered to have mild curvature when $\delta/R \leqslant 0.01$, where δ is the thickness of the wall layer within which the mean velocity is less than 99% of the free-stream velocity, U_∞, and R is the radius of curvature at the wall (Bradshaw 1973). In a homogeneous shear flow there is no counterpart to the boundary-layer thickness. As mentioned earlier, however, a representative measure of curvature is the parameter S. This parameter would, generally, vary across a boundary layer but, if one were to make the crude assumption $\mathrm{d}U/\mathrm{d}n \sim O(U_\infty/\delta)$, then $\delta/R \sim O(S)$. The maximum shear that can be generated by the existing facility corresponds to a flow-generator constant $k_s = (1/U_c)(\mathrm{d}U/\mathrm{d}n) = 6.5\ \mathrm{m}^{-1}$ (TK). As mild curvature for this flow, a curved section with a centreline radius $R_c = 5$ m was chosen, which, in the unobstructed shear flow and depending upon the orientation of the shear generator, resulted in the values $S \approx \pm 0.03$. Following the procedure introduced by KT, flows with smaller values of k_s and, hence, larger magnitudes of S could be created by placing uniform obstructions in the flow. The second curved section had a smaller centreline radius, $R_c = 2$ m, giving $S \approx \pm 0.08$ in the unobstructed flow. Higher values of S in this section were also obtained by decreasing k_s using flow obstructions. The use of two different curved sections permitted the generation of flows with a wide range of S values and the study of flow structure dependence upon the magnitudes of k_s and R_c separately. Flows generated in the two curved sections had overlapping ranges of S.

The length of the curved sections was chosen with the objective of allowing adequate development of the turbulence, at least for the high-shear cases. In the high-shear, straight flow, the turbulence became self-preserving within 2 m of the flow separator for the centreline speeds of interest here. By analogy, the lengths of the

Grid/screen symbol	Type	σ	M_g (mm)	d (mm)
G	parallel grid	0.38	25.4	9.75
S1	woven screen	0.26	12.7	1.76
S2	woven screen	0.29	3.2	0.70
S3	woven screen	0.29	3.2	0.70

TABLE 1. Specifications for the grid and screens used in the present study (d is the grid/screen element diameter)

Case	$x_g = 0$ m	$x_g = 0.32$ m	$x_g = 0.76$ m	$x_g = 1.37$ m	x_{gi} (m)
A	—	—	—	—	0
B	S2	—	—	—	0
C	S1	S2	—	—	0.32
D	G	S1	S2	—	0.76
E	G	S1	S2	S3	1.37

TABLE 2. Positions of various grids and screens used to produce the shear flows

curved sections were chosen to be about 2 m. It may be noted that this is a rather conservative estimate, because the flow disturbance introduced by the change from a straight section to a curved one should be much weaker than that due to flow passage through the shear generator. The height, h_c, of the curved sections was 65 mm smaller than the height of the upstream straight section. Similarly, there was a 47 mm width reduction from the straight to the curved sections. The objective of these reductions was to remove the boundary layers at the entrance of the curved sections, in order to reduce wall effects in the core region of the curved flows.

5.2. *Generation of shear*

The objective of the design of the apparatus used was to generate curved shear flows with different values of the parameter S. Note first that a measurable change in S would not be produced by changing the tunnel speed, U_c, because that would result in flows with essentially the same values of k_s (KT, TK). Flows with lower values of k_s could, however, be produced by inserting a number of screens and/or grids normal to the flow downstream of the shear generator (KT). In order to facilitate comparisons of the results, the combinations of inserted screens and/or grids were selected such that, at the entrance to the curved section, all flows would have comparable values of the turbulent intensities and lengthscales. While the solidity, σ, of these obstructions determines k_s, the intensity and lengthscales of the turbulence are also influenced by the spacing or mesh size, M_g, and the positioning, x_g of the obstructions. Three woven screens and one grid of parallel rods were combined to produce five sets of flow conditions (tables 1 and 2) with $0.53 < k_s < 6.25$. These flows will be referred to as cases A–E. Flows with roughly the same magnitudes but opposite directions of shear were achieved by inverting the shear generator. Therefore, a total of ten flow conditions could be generated; these will be referred to as NA–NE and PA–PE respectively (N stands for 'negative' and P for 'positive' shear). In the straight tunnel the orientation of the shear is unimportant and any difference in the measured development of the turbulence between, for example, cases NA and PA can be attributed mainly to asymmetries of the shear generator and

screens, misalignment of the wind tunnel components and measurement errors. In the curved flow, however, the orientation of shear with respect to the curvature is an important factor that influences the development of turbulence.

5.3. *Instrumentation and measuring procedures*

All measurements in the present study were performed with hot-wire anemometers, using a custom-made, cross-wire array (TSI 1248BJT15). The sensing elements were made of tungsten and had a diameter of 5 μm and a length of 1.2 mm. They were separated by 0.5 mm and had nominal inclinations of $\pm 45°$ with respect to the axis of the probe body. The wires were powered by constant-temperature bridges (TSI 1050A) and operated at an overheat ratio of about 1.5.

The hot wires were calibrated in the wind tunnel, with all flow obstructions removed to provide a low-turbulence airstream ($u'/U \approx 0.005$). The bridge voltage for each wire was related to the instantaneous velocity using a modified form of King's law, with coefficients adjusted by least-squares fitting to the calibration data. To condition the hot-wire signals for digitization, an analog electronic circuit was used to offset, amplify (gain of 20) and low-pass filter (cutoff frequency of 10 kHz) the input signals. All signals were digitized using a 12-bit analog to digital converter (Data Translation DT 2828), connected to a micro-computer. The analog to digital converter had a ± 10 V range, giving a nominal resolution of 5 mV.

The sidewalls of the curved sections were engraved with a polar coordinate system and the probe tip was positioned by aligning it with the corresponding lines on the two tunnel walls. The maximum error in the streamwise positioning of the probe was about 2 mm. The axis of the probe body was positioned by eye, tangentially to both the centreplane of the tunnel and the engraved, circular coordinate at each streamwise location. The maximum error of this positioning was about 1° in the (s, n)-plane and about 3° in the (s, z)-plane. Because the turbulent fields in the present flows were nearly homogeneous but strongly anisotropic, the measurements would be relatively insensitive to errors in probe translation but very sensitive to pitching of the probe. An empirical study in which the probe was pitched in the (s, n)-plane, suggests that a 1° error in alignment would lead to 1% error in $\overline{u^2}$, a 2% error in $\overline{v^2}$ and a 5% error in $\overline{uv}$. The accuracy in the measurement of U would not be significantly affected by slight misalignment but the error in V could exceed 100%.

The streamwise integral lengthscales, L_{uu}, L_{vv} and L_{ww}, of the streamwise, transverse and spanwise velocity fluctuations were measured by integrating the corresponding autocorrelation coefficients to their first zeros and using Taylor's 'frozen flow' approximation. The streamwise Taylor microscales, λ_u, λ_v and λ_w, were measured as

$$\lambda_u = [\overline{u^2}/(\overline{\partial u/\partial s})^2]^{\frac{1}{2}}, \tag{30}$$

$$\lambda_v = [2\overline{v^2}/(\overline{\partial v/\partial s})^2]^{\frac{1}{2}}, \tag{31}$$

$$\lambda_w = [2\overline{w^2}/(\overline{\partial w/\partial s})^2]^{\frac{1}{2}}, \tag{32}$$

where the streamwise derivatives were estimated from the corresponding temporal derivatives using Taylor frozen flow approximation.

6. Measurements in the straight section

The characteristics of the straight flows, measured with a curved section in place, are summarized in tables 3, 4 and 5. The values of certain parameters were slightly different from those reported by TK, presumably owing to minor adjustments of the

Case	U_c (m/s)	dU/dn (s^{-1})	k_s (m^{-1})
NA	10.3	−64	6.3
NB	9.8	−50	5.1
NC	10.0	−30	3.0
ND	9.9	−15	1.5
NE	9.4	−5	0.6
PA	9.7	65	6.7
PB	9.6	53	5.5
PC	9.8	29	3.0
PD	9.7	13	1.3
PE	9.4	5	0.5

TABLE 3. The mean flow conditions at the end of the straight section

Case	τ_0	$\overline{q_0^2}$ (m^2/s^2)	κ_q	L_{uu0} (mm)	m_s	m_τ	κ_L	λ_{u0} (mm)	$\frac{\lambda_v}{\lambda_u}$	$\frac{\lambda_w}{\lambda_u}$
NA	20.0	1.31	0.083	46	0.015	0.093	0.076	5.4	0.73	0.83
NB	16.0	0.60	0.073	32	0.0096	0.074	0.081	5.6	0.73	0.83
NC	8.6	0.17	0.11	26	0.0046	0.061	0.071	7.0	0.79	0.86
ND	3.7	0.57	0.069	100	0.012	0.30	0.085	9.9	0.71	0.79
NE	1.0	0.10	—	82	0.015	1.8	0.63	10.3	0.91	1.00
PA	21.4	1.70	0.098	46	0.015	0.089	0.070	5.4	0.73	0.81
PB	17.8	0.66	0.072	32	0.0086	0.061	0.065	5.3	0.75	0.85
PC	8.6	0.18	0.14	26	0.0046	0.059	0.068	6.7	0.81	0.85
PD	3.2	0.48	0.083	103	0.021	0.63	0.18	9.4	0.75	0.85
PE	1.0	0.11	—	78	0.013	1.0	0.38	9.9	0.99	1.05

TABLE 4. Reference values of turbulent parameters at the end of the straight section

Case	Re_L ($u'L_{uu}/\nu$)	L_{uu}/l	Re_λ ($u'\lambda_u/\nu$)	P^*	$\frac{\frac{1}{2}\kappa_q}{P^*}$	$\frac{\epsilon_i^*}{P^*}$	$\frac{\epsilon_b^*}{P^*}$
NA	2080	2.2	280	0.143	0.29	0.84	0.71
NB	1030	2.1	190	0.150	0.24	0.93	0.76
NC	450	1.9	130	0.147	0.38	0.95	0.62
ND	3140	2.0	340	0.156	0.22	0.96	0.78
NE	1040	1.4	140	0.168	—	—	1.0
PA	2430	2.3	310	0.135	0.36	0.89	0.64
PB	1080	2.1	190	0.133	0.27	1.05	0.73
PC	470	1.8	130	0.133	0.51	1.20	0.49
PD	3150	1.9	300	0.140	0.30	1.29	0.70
PD	1010	1.2	130	0.134	—	—	—

TABLE 5. Estimated values of dimensionless parameters at the end of the straight section

shear generator, the aging of the system and differences in the measuring techniques. The dimensionless time (total strain) in the straight section is defined as

$$\tau = \frac{x_s - x_{g1}}{U_c}\left|\frac{dU}{dn}\right|, \tag{33}$$

where x_{g1} is the position of the farthest downstream obstruction used for the generation of a particular flow. The symbol τ_0 denotes the value of τ at the exit of the straight section, just before the entrance to the curved section and the symbol $\overline{q_0^2}$ represents the value of turbulent kinetic energy obtained by exponential extrapolation of the measurements to the end of the straight section. Plots of various flow properties in the straight section will be presented together with those in the curved sections.

Previous investigators have proposed that, in rectilinear, uniformly sheared flow, the integral lengthscales would grow linearly or exponentially. We have considered both possibilities by least-squares fitting of appropriate functions to the measurements, as

$$\frac{L_{uu}}{M} = m_s\frac{x_s - x_{s0}}{M} + \frac{L_{uu0}}{M}, \tag{34}$$

$$\frac{L_{uu}}{M} = m_\tau(\tau - \tau_0) + \frac{L_{uu0}}{M}, \tag{35}$$

$$\frac{L_{uu}}{L_{uu0}} = e^{\kappa_L(\tau-\tau_0)}, \tag{36}$$

where L_{uu0} represent values extrapolated from the measurements to the end of the straight tunnel (differences between linear and exponential extrapolations can be neglected in the present context), corresponding to a downstream position x_{s0} and a dimensionless time τ_0. Best fits of the three coefficients m_s, m_τ and κ_L are given in table 4. Although most data appear to be best described by the exponential law, variations in the values of the three coefficients for different flows indicate that, unlike grid turbulence, uniformly sheared flows may not obey a universal law for scale evolution.

The five straight shear flows used here (flows with positive and negative shear are considered identical in this context) could perhaps be divided into what has previously been referred to as high-shear or low-shear flows (Harris *et al.* 1977). Cases A, B and C would be considered as high-shear flows, as they result in growing stresses and integral scales. Cases D and E could be considered as low-shear flows, having constant or decaying stresses and growing integral scales; they are comparable to the experiments of Champagne *et al.* (1970) and cases O and P of TK. Careful examination of the development of K_{uu}, K_{vv}, K_{ww} and K_{uv} with τ has revealed that only cases A, B and C could confidently be considered as having achieved, before the end of the straight section, near constancy of these dimensionless stresses. For these cases, the dimensional stresses appeared to grow exponentially. For cases D and E, the dimensionless stresses were still changing at the end of the straight section, while the dimensional ones had not started to grow.

Tests of self-preservation, based on the constancy of non-dimensionalized integral lengthscales, have been presented by Harris *et al.* (1977) and by TK, who found that the 'turbulence Reynolds number:', $R_T = (dU/dn)^2 L_{uu}^2/K_{uv}\overline{q^2}$, evaluated for all

published data grew slightly with τ. The present measurements show that, in all cases, the lengthscale ratio L_{uu}/l (and, consequently, R_T) changed relatively little compared to the change of either $\overline{q^2}$ or L_{uu}. The fact that this ratio maintained a value of order one in all cases is consistent with the expectation that turbulence production was dominated by shearing effects.

Estimates of the dimensionless kinetic energy dissipation rate, ϵ_b^*, can be based on the balance of the production and convection terms in (12). Such estimates have been presented for a variety of uniformly sheared flows by TK, using the notation τ_s/τ_e. Alternatively, the development of ϵ^* could also be estimated from the isotropic relation

$$\epsilon_i^* = 30\nu \frac{K_{uu}}{|\mathrm{d}U/\mathrm{d}n|\,\lambda_u^2}. \tag{37}$$

Both estimates are presented in table 5, which shows the systematic relation $\epsilon_b^* < \epsilon_i^*$. The values of ϵ_i^* seemed to achieve approximate constancy near the end of the straight section, in cases A, B, C and D, while they showed a persisting change in case E.

As table 5 shows, for those flows which demonstrated a self-preserving character, dimensionless statistics spanned relatively narrow ranges of values, although shear rates differed substantially. Nevertheless, considering that all these flows were generated by similar means, it is not possible to conclude with certainty whether these dimensionless statistics approached values which were independent of the flow facility and, thus, inherent to uniformly sheared turbulence.

The straight shear flows A, B and C had length and velocity scales with comparable magnitudes and rates of growth; the somewhat higher kinetic energy growth rate in case C could, perhaps, be accommodated by considering that, in this case, the last obstruction was a fine mesh screen and not a larger mesh grid or flow separator as in the other cases. The structures of these flows were effectively identical, as indicated by the comparable asymptotic values of the dimensionless turbulent stresses and lengthscales. In any case, the differences in growth rates and in structural parameters among cases A, B and C in the straight section are sufficiently small to permit an evaluation of the effects of curvature by a direct comparison of their developments in the curved sections.

The low-shear flows, D and E, were subject to relatively small values of total strain in the straight section and, as a result, their structure did not appear to have reached its asymptotic state. Furthermore, the small value of shear introduced a higher uncertainty in the determination of the total strain and the evolution rates. On the other hand, cases D and E exhibited the highest values of S, and, therefore, were affected by curvature much more than the high-shear cases. For these reasons, results from cases D and E will be used for a qualitative assessment of strong curvature effects but not in the quantitative analysis of the results.

7. Measurements in the curved sections

7.1. *Mean velocity*

Tables 6 and 7 present measurements of shear rates and centreline velocities for the different flows at two locations, one near the entrance to each curved section and one near its exit. In general, the former values were representative of conditions in the major part of the test section and will thus be used in the following. In any case, it

	$s/h_c = 0.417$				$s/h_c = 5.42$			
Case	U_c (m/s)	dU/dn (s^{-1})	k_s (m^{-1})	S	U_c (m/s)	dU/dn (s^{-1})	k_s (m^{-1})	S
NA	10.2	−61	6.0	−0.033	10.6	−51	4.8	−0.042
NB	9.8	−50	5.1	−0.039	9.8	−46	4.7	−0.043
NC	9.9	−30	3.0	−0.066	10.0	−26	2.6	−0.077
ND	9.8	−16	1.6	−0.12	9.7	−11	1.1	−0.17
NE	9.5	−6	0.6	−0.3	9.5	−6	0.7	−0.3
PA	10.1	64	6.3	0.032	10.1	61	6.0	0.033
PB	10.3	52	5.0	0.040	10.3	50	4.9	0.041
PC	10.3	27	2.6	0.076	10.3	26	2.5	0.079
PD	10.4	11	1.1	0.19	10.5	9.5	0.9	0.22
PE	9.6	3	0.3	0.6	9.9	2	0.2	1

TABLE 6. The mean flow conditions in the mildly curved section ($R_c = 5$ m)

	$s/h_c = 0.417$				$s/h_c = 4.74$			
Case	U_c (m/s)	dU/dn (s^{-1})	k_s (m^{-1})	S	U_c (m/s)	dU/dn (s^{-1})	k_s (m^{-1})	S
NA	10.1	−64	6.3	−0.079	11.4	−60	5.3	−0.095
NB	9.7	−52	5.4	−0.093	10.0	−54	5.4	−0.093
NC	9.6	−31	3.2	−0.15	10.3	−31	3.0	−0.17
ND	9.6	−19	2.0	−0.25	10.4	−17	1.6	−0.31
NE	9.1	−9	0.9	−0.5	9.7	−9	0.9	−0.5
PA	10.1	65	6.4	0.078	10.5	64	6.1	0.082
PB	10.6	53	5.0	0.10	10.8	52	4.8	0.10
PC	11.0	30	2.7	0.18	11.0	30	2.7	0.18
PD	10.2	8	0.8	0.64	11.2	9	0.8	0.62
PE	9.6	< 1	< 0.1	> 5	10.4	< 1	< 0.1	> 5

TABLE 7. The mean flow conditions in the strongly curved section ($R_c = 2$ m)

can be seen that the variation of the mean velocity along the centreline of the curved sections was less than 3% and that the mean shear was effectively constant, with the possible exception of the near-exit region of the tunnel, particularly in some negatively sheared cases. The transverse and spanwise mean velocity components were generally found to be smaller than 1% of U_c. In most cases the mean shear had spanwise variations that were comparable to those in previous experiments in rectilinear shear flows. In some cases with a negative shear, however, the spanwise uniformity of the shear deteriorated near the end of the section, although in a manner which did not appear to be related to the boundary-layer growth.

Upon entering the curved section, the mean shear magnitude appeared to decrease somewhat when $S > 0$, and to increase when $S < 0$. This observation is compatible with the concept of conservation of vorticity in inviscid flow and the fact that, although in the straight section the vorticity happens to be equal to the mean shear, in the curved section it is equal to the sum $dU/dn + U/R$.

7.2. *Presentation of turbulence measurements*

To assist future work, we wish to present as many direct measurements of primary turbulent quantities as possible, and in view of the large volume of measurements obtained, we summarize here the approach followed in the presentation of these results. First, because it was found that the degree of transverse inhomogeneity of the Reynolds stresses in the curved sections was generally comparable to that in straight shear flows (TK; although somewhat more pronounced in the $S < 0$ cases), only measurements along the tunnel centreline will be presented. In anticipation of exponential evolution of the turbulent stresses and lengthscales, these quantities will be plotted *vs.* the dimensionless evolution time (total strain) in semi-logarithmic coordinates. All measurements of a certain quantity corresponding to flows with roughly the same mean shear will be presented in the same plot. These include two flows in the straight section and a pair of flows in each of the curved sections. Therefore, each turbulent parameter will be presented in a set of five plots, each containing six sets of measurements. It is noted that, in the straight section, τ will be defined according to (33), whereas, in the curved sections, it will be defined as

$$\tau = \tau_0 + \frac{s}{U_c}\left|\frac{\mathrm{d}U}{\mathrm{d}n}\right| \tag{38}$$

To avoid confusion among different cases, the measurements will be plotted *vs.* $\tau - \tau_0$, with the understanding that negative values of this parameter correspond to the straight section, while positive ones correspond to a curved section.

For economy of presentation, the downstream evolution of turbulent activity will be represented by plots of the kinetic energy, $\overline{q^2}$, the streamwise integral lengthscale, L_{uu}, and the streamwise Taylor microscale, λ_u (all normalized by the corresponding values at the entrance to the curved section), while the evolution of the turbulence structure will be represented by plots of the anisotropy of the dimensionless Reynolds stress, defined as

$$m_{uu} = K_{uu} - \tfrac{1}{3}, \quad m_{vv} = K_{vv} - \tfrac{1}{3}, \quad m_{ww} = K_{ww} - \tfrac{1}{3}, \quad m_{uv} = K_{uv},$$

and the anistropy of the integral lengthscale ratios, $2L_{vv}/L_{uu} - 1$ and $2L_{ww}/L_{uu} - 1$.

The curved shear flows can be separated into two distinct classes, the destabilized ones, i.e. those with $S < 0$, and the stabilized ones, i.e. those with $S > 0$. There is also a distinction between the high-shear (cases A, B and C) and the low-shear (cases D and E) flows. Presentation of the measurements will be made following this classification. Note that, when comparing the evolution rates between flows with different shear, one must consider the differences in the ranges of the horizontal axes.

7.3. *Turbulent kinetic energy and its partition*

Measurements of the turbulent kinetic energy along the centreline of the wind tunnel, comprising the straight section and either of the two curved sections, are plotted against the (offset) dimensionless time, $\tau - \tau_0$, in figure 3, while the measured anisotropies of the Reynolds stress tensor are plotted *vs.* $\tau - \tau_0$ in figure 4. The kinetic energy measurements were fitted with an exponential function and the evolution coefficients, κ_q, evaluated for each flow using linear regression on the semi-logarithmic axes, are presented in table 8.

Inspection of figure 3 reveals that, universally and unmistakeably, curvature enhanced the evolution rate of turbulent kinetic energy when $S < 0$ and it suppressed it when $S > 0$. For the same entrance conditions, this enhancement or supression was always stronger in the strongly curved section than in the mildly curved section.

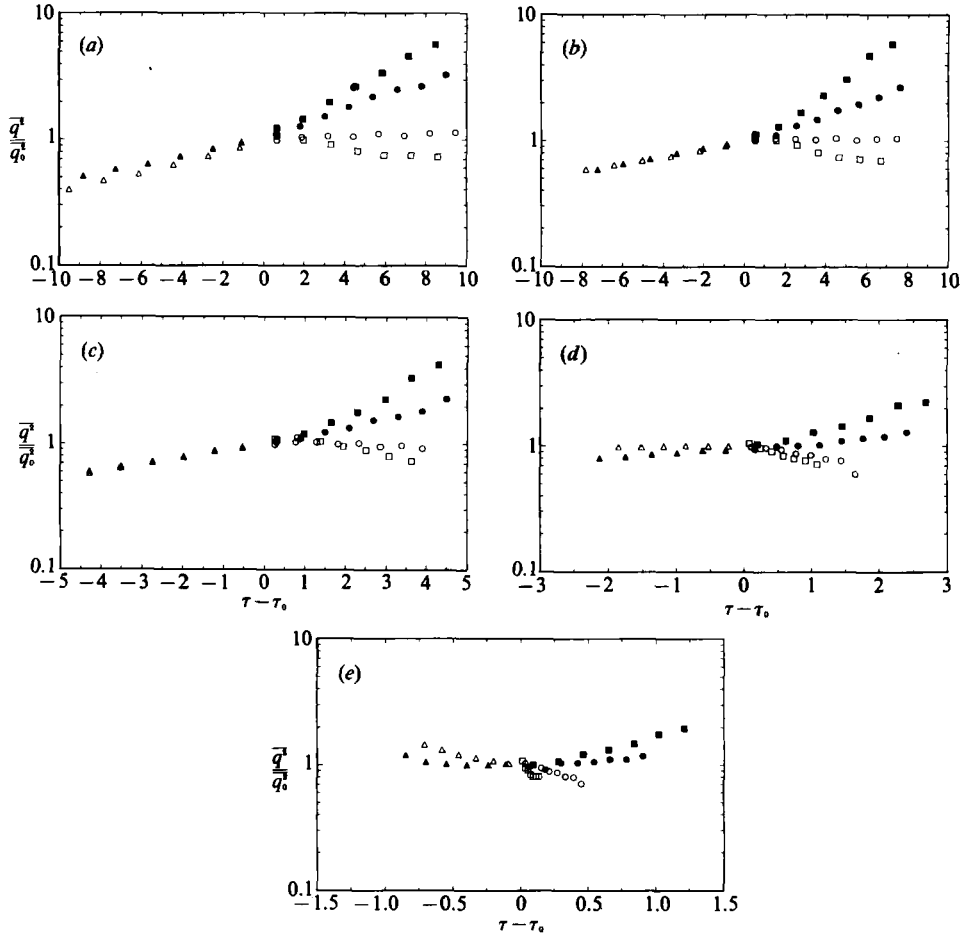

FIGURE 3. Evolution of the turbulent kinetic energy along the wind tunnel centreline for flow types A (*a*), B (*b*), C (*c*), D (*d*) and E (*e*); triangles signify results in the straight section, circles in the mildly curved section and boxes in the strongly curved section; open symbols indicate positive S and closed symbols negative S.

In all destabilized ($S < 0$) flows, the turbulent kinetic energy grew nearly exponentially in the curved sections, even in case NE, for which exponential growth had not been established at the end of the straight section. The enhancement for a given shear rate was always greater in the strongly curved section and the coefficient κ_q appeared to increase monotonically with increasingly negative S. As indicated by the near constancy of the Reynolds stress anisotropies away from the two ends of the curved sections, in the high-shear cases, NA, NB and NC, the turbulence structure appeared to reach self-preserving states that were practically independent of τ. In the low-shear cases, ND and NE, however, some anisotropies were monotonically developing downstream, indicating that self-preservation of the turbulence structure had not yet been attained at the last measuring station. Of course, these observations are consistent with the fact that high-shear flows were more 'mature' than the low-shear ones, the former having been subjected to much larger total strains than the latter; similar observations were made for these flows in the straight section. Among the low-shear cases, ND was the closest to full development when it entered the

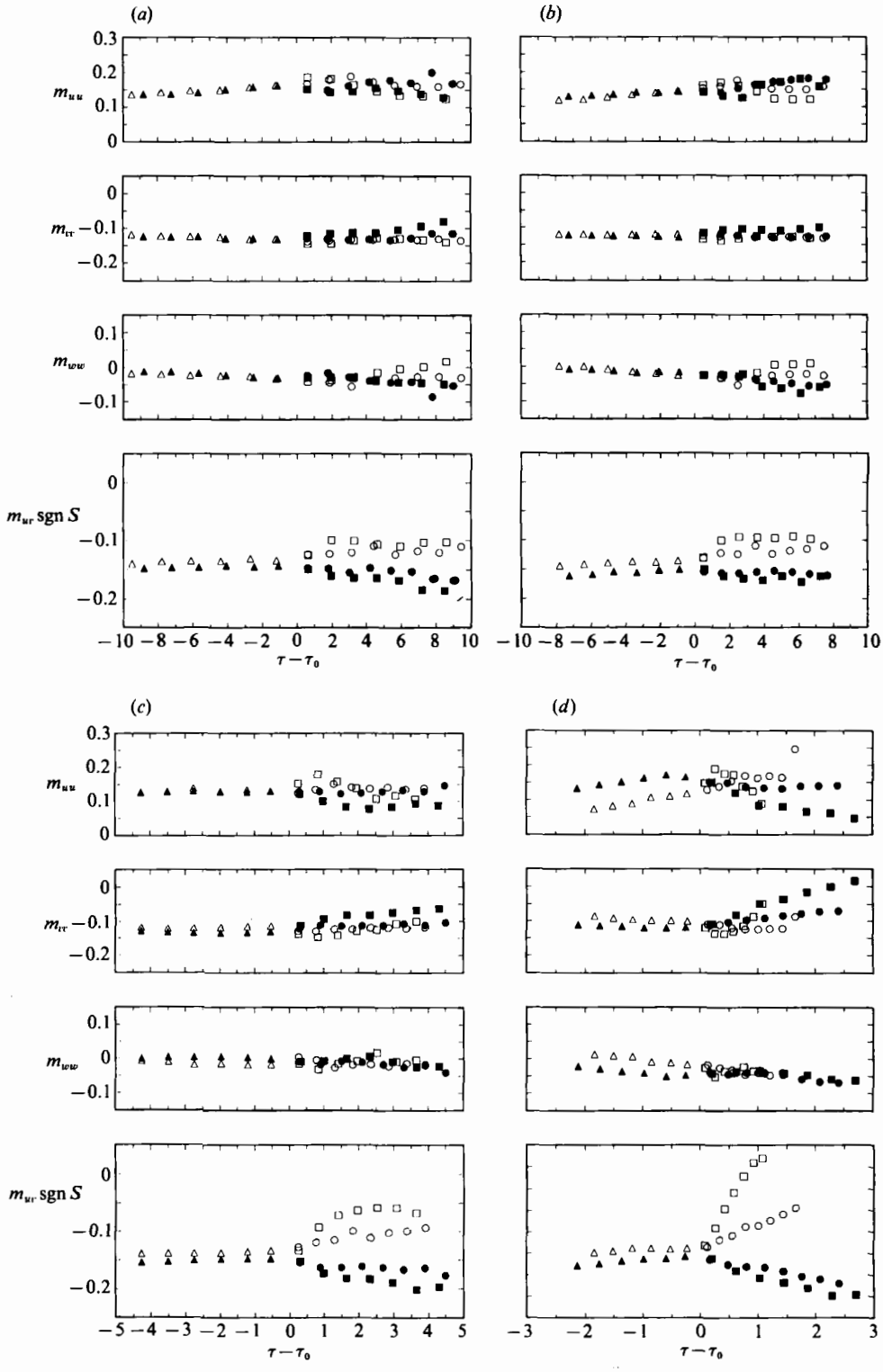

FIGURE 4 (*a–d*). For caption see facing page.

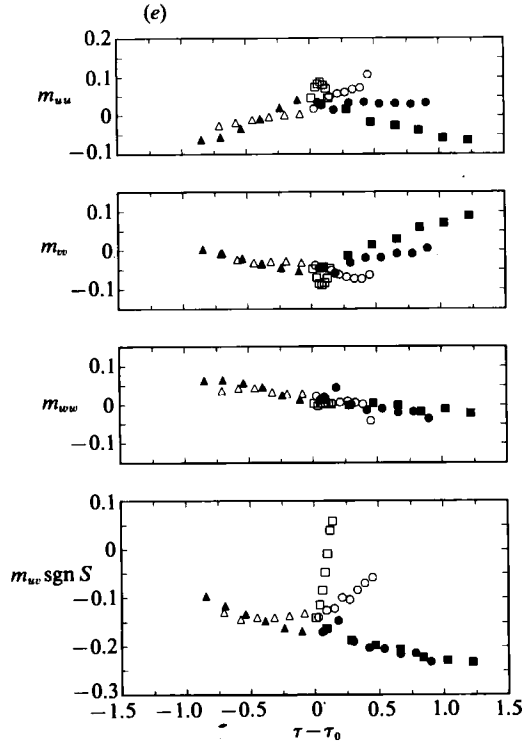

FIGURE 4. Evolution of the anisotropy of the Reynolds stresses along the wind tunnel centreline. Cases and symbols as in figure 3.

	$R_c = 5$ m				$R_c = 2$ m			
Case	κ_q	m_s	m_τ	κ_L	κ_q	m_s	m_τ	κ_L
NA	0.132	0.025	0.17	0.073	0.204	0.048	0.29	0.104
NB	0.136	0.022	0.17	0.100	0.256	0.043	0.32	0.148
NC	0.191	0.0086	0.11	0.095	0.342	0.019	0.23	0.166
ND	0.145	0.028	0.68	0.148	0.327	0.048	0.95	0.196
ND	0.270	0.013	0.87	0.193	0.590	0.025	1.1	0.318
PA	0.015	0	0	0	−0.053	−0.016	−0.097	−0.065
PB	0.004	0	0	0	−0.076	−0.007	−0.052	−0.049
PC	−0.020	0	0	0	−0.126	−0.006	−0.093	−0.105
PD	−0.268	−0.007	−0.24	−0.076	−0.379	−0.036	−1.76	−0.59
PE	−0.791	—	—	—	—	—	—	—

TABLE 8. Turbulence evolution coefficients in the curved sections

curved section and reached the largest total strain within it. Even so, case ND in the mildly curved section had a substantially lower exponent of growth of $\overline{q^2}$ than case NB had in the strongly curved section, although the two flows had comparable values of S.

Among the stabilized ($S > 0$) flows, case PA in the mildly curved section exhibited a weak growth of kinetic energy, and case PB, also in the mildly curved section, maintained a nearly constant level of $\overline{q^2}$, while, in all other cases, the kinetic energy

S	ρ	$\frac{\overline{u^3}}{\overline{u'^3}}$	$\frac{\overline{v^3}}{\overline{v'^3}}$	$\frac{\overline{w^3}}{\overline{w'^3}}$	$\frac{\overline{u^2v}}{\overline{u'^2v'}}$	$\frac{\overline{uv^2}}{\overline{u'v'^2}}$	$\frac{\overline{u^2w}}{\overline{u'^2w'}}$	$\frac{\overline{uw^2}}{\overline{u'w'^2}}$	—	—
−0.10	0.50	−0.141	−0.063	−0.100	−0.051	−0.061	0.016	0.001	—	—
0.10	−0.30	−0.051	0.053	−0.003	0.037	−0.037	0.002	−0.021	—	—
Gaussian	—	0	0	0	0	0	0	0	—	—
S	ρ	$\frac{\overline{u^4}}{\overline{u'^4}}$	$\frac{\overline{v^4}}{\overline{v'^4}}$	$\frac{\overline{w^4}}{\overline{w'^4}}$	$\frac{\overline{u^3v}}{\overline{u'^3v'}}$	$\frac{\overline{u^2v^2}}{\overline{u'^2v'^2}}$	$\frac{\overline{uv^3}}{\overline{u'v'^3}}$	$\frac{\overline{u^3w}}{\overline{u'^3w'}}$	$\frac{\overline{u^2w^2}}{\overline{u'^2w'^2}}$	$\frac{\overline{uw^3}}{\overline{u'w'^3}}$
−0.10	0.50	2.94	3.14	3.13	1.42	1.49	1.44	−0.168	1.03	−0.176
Gaussian	—	3	3	3	1.5	1.5	1.5	0	1.0	0
0.10	−0.30	2.99	3.28	3.17	−0.911	1.22	−0.945	−0.128	0.999	−0.128
Gaussian	—	3	3	3	−0.9	1.18	−0.9	0	1.0	0

TABLE 9. Typical values of higher-order moments in a curved shear flow (case B, $s/h_c = 3.0$, $R_c = 2$ m)

decayed downstream. Although exponential evolution of $\overline{q^2}$ cannot be established with certainty, because of its small change in the curved sections, exponential curves were also fitted to these measurements, in order to permit a direct comparison of all cases. The resulting values of κ_q were, respectively, positive (in the mildly curved PA), near zero (in the mildly curved PB) and negative (in all other cases) and generally decreased with increasing S. As in the destabilized cases, the downstream development of the Reynolds stress anisotropy reveals an attainment of self-preserving structures for the high-shear cases, PA, PB and PC, but not for the low-shear cases, PD and PE.

The anisotropies of the normal stresses were subject to some scatter, part of which may be because the spanwise stress was measured separately from the other two. Although every effort was made to align locally the hot-wire probe body with the tunnel centreline, the sensitivity of these stresses to probe orientation may have also introduced some uncertainty. In any case, the high-shear results cannot reveal any systematic effect of curvature upon the anisotropies of the normal stresses. On the other hand, the low-shear results show a tendency of negative curvature ($S < 0$) to reduce the streamwise dimensionless stress, K_{uu}, and to increase the transverse dimensionless stress, K_{vv}, while positive curvature ($S > 0$) had the opposite effects. The spanwise dimensionless stress, K_{ww}, appeared to be unaffected by curvature and maintained the nearly isotropic value that it developed in the straight section. Therefore, one may conclude that its effects upon the normal stress anisotropies may be neglected in cases of weak curvature.

Higher-order moments of the three components of velocity in the curved shear flow had nearly Gaussian values with deviations that were, generally, compatible with the level of inhomogeneity. Typical values are shown in table 9.

7.4. *Turbulent shear stress*

Among all measured dimensionless quantities (see table 10), it was the dimensionless shear stress, K_{uv} (which is equal to its anisotropy, m_{uv}), that appeared to be most sensitive to curvature. All measurements of this parameter illustrated very consistently that, while mean shear tended to produce a shear stress opposite to its direction, curvature tended to produce a shear stress directed away from the centre of curvature. When the directions of the two production mechanisms coincided (i.e.

Case	S	K_{uu}	K_{vv}	K_{ww}	$-K_{uv} \times \operatorname{sgn} S$	$\frac{L_{uu}}{l}$	$\frac{\lambda_u}{\lambda_{u0}}$	P^*	$\frac{\frac{1}{2}K_q}{P^*}$	$\frac{\epsilon_1^*}{P^*}$	$\frac{\epsilon_b^*}{P^*}$
NA (M)	−0.033	0.51	0.20	0.29	0.150	2.3	1.09	0.155	0.43	0.70	0.67
NB (M)	−0.039	0.51	0.20	0.29	0.155	2.4	1.09	0.161	0.42	0.77	0.58
NC (M)	−0.066	0.46	0.22	0.32	0.164	1.8	0.95	0.175	0.55	0.89	0.45
NA (S)	−0.079	0.50	0.23	0.27	0.167	2.5	1.14	0.180	0.57	0.52	0.43
NB (S)	−0.093	0.48	0.23	0.29	0.165	2.5	1.15	0.180	0.71	0.56	0.29
NC (S)	−0.15	0.42	0.25	0.33	0.192	1.9	0.99	0.221	0.77	0.57	0.23
PA (M)	0.032	0.48	0.20	0.32	0.117	2.1	1.01	0.113	0.066	1.0	0.93
PB (M)	0.040	0.50	0.19	0.31	0.112	2.0	1.00	0.108	0.019	1.4	0.98
PC (M)	0.076	0.47	0.21	0.32	0.102	1.6	0.90	0.094	−0.11	2.3	1.1
PA (S)	0.078	0.46	0.20	0.34	0.104	1.9	0.98	0.096	−0.28	1.2	1.3
PB (S)	0.10	0.47	0.19	0.34	0.096	1.8	0.97	0.086	−0.44	1.8	1.4
PC (S)	0.18	0.45	0.21	0.34	0.061	1.4	0.86	0.050	−1.3	4.1	2.3

TABLE 10. Some dimensionless parameters for curved, high-shear flows (M indicates mildly curved and S strongly curved)

when $S < 0$), the quantity $m_{uv} \operatorname{sgn} S$ tended to decrease from its negative value in the straight section, and, when these directions opposed each other (i.e. when $S > 0$), that quantity increased. The changes in shear stress anisotropy were consistently larger in the strongly curved section than in the mildly curved one.

In the high-shear flows, the dimensionless shear stress quickly reached nearly constant asymptotes, whose values decreased systematically with increasing S. In the low-shear flows, however, the same quantity maintained a monotonic variation throughout the curved sections, in which, as mentioned earlier, only modest or small (especially in the PE cases) total strains were achieved. Comparing the four low-shear cases separately, one may conclude that the ND and NE cases were closer to an asymptotic structure at the exit of the curved section than cases PD and PE were. The strongly curved PD and PE cases, in particular, show spectacular increases of $m_{uv} \operatorname{sgn} S$ from its initial negative levels, across zero, to positive values, with all indications pointing to even larger positive asymptotic levels, if one presumes that self-preserving states were to be attained given additional tunnel length; of course, growth of this quantity cannot persist indefinitely, as it is statistically bounded by an upper bound that is less than unity. A reversal in direction of shear stress, such as to achieve the same sign as the mean shear has previously been observed only in strongly inhomogeneous flows. This phenomenon appeared for values of S that were of order unity, in which case curvature effects are expected to dominate over those of shear. Nevertheless, because shear and curvature effects are inherently coupled through the governing equations, it is not clear whether initially sheared flow subjected to curvature would attain the same asymptotic structure as initially unsheared curved flow would.

7.5. *Integral lengthscales*

The streamwise evolution of the streamwise integral lengthscale, L_{uu}, in both the straight and the curved sections, are plotted in semi-logarithmic coordinates *vs.* $\tau - \tau_0$ in figure 5. In a fashion similar to that of the turbulent kinetic energy evolution, the growth of this scale in the straight section was enhanced by negative curvature ($S < 0$) and suppressed by positive curvature ($S > 0$). This effect was manifested in a stronger way in the strongly curved section than in the mildly curved one. Most

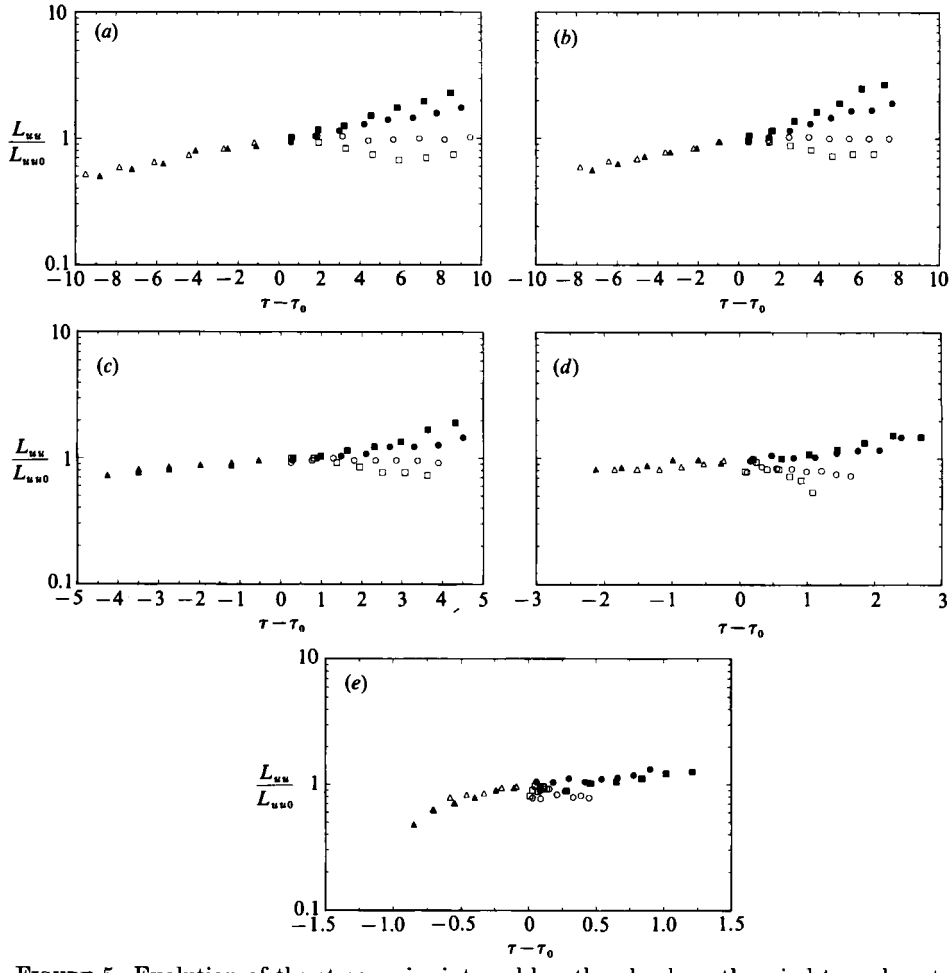

FIGURE 5. Evolution of the streamwise integral lengthscale along the wind tunnel centreline. Cases and symbols as in figure 3.

lengthscale measurements (excluding data near the two ends of the curved sections and flows with 'immature' structures) were compatible with fitted exponential curves, in which the evolution coefficient, κ_L could be positive, near zero or negative. These coefficients, as well as optimum coefficients, m_s and m_τ, for linear fits according to (34)–(36), are presented in table 8. Note the contrast between the present cases with very weak turbulence production (large positive S), in which both the turbulent kinetic energy and the lengthscales decrease downstream, and grid turbulence, in which the turbulent kinetic energy decays but the lengthscales grow downstream.

The effect of curvature on the relative evolution of velocity and lengthscales is presented in figure 6, in the form of plots of the ratio L_{uu}/l *vs.* $\tau-\tau_0$, where l is defined by (11). This ratio is proportional to the ratio of the mean shear timescale, $(\mathrm{d}U/\mathrm{d}n)^{-1}$, and the turbulent 'eddy turnover' time, L_{uu}/u', used by TK. In the mature flows in the straight section, the ratio L_{uu}/l varied only slightly from a value around 2.0, in conformity with the measurements presented by TK. The effect of curvature was to increase this ratio when $S<0$ and to decrease it when $S>0$, the more so, the larger the magnitude of S. This is particularly obvious in the PD and PE cases, especially

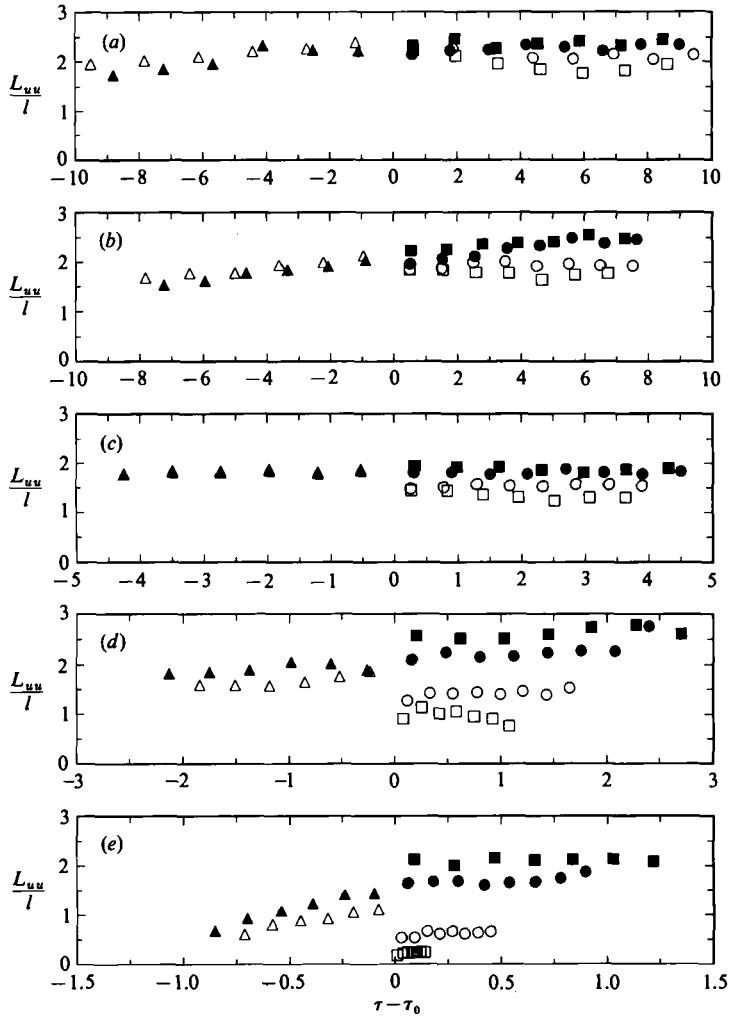

FIGURE 6. Evolution of the dimensionless turbulence scale, L_{uu}/l. Symbols as in figure 3.

in the strongly curved section. Based on these observations, one may conclude that, although in rectilinear shear flows the mean shear imposes its own timescale on the turbulence structure, in curved shear flows the temporal evolution of this structure is influenced by both the shearing and the curvature timescales. Unfortunately, a quantitative description of this phenomenon is not possible, because the flows that exhibited the strongest curvature effects did not reach an asymptotic structure in the present facility.

As additional indicators of the effects of curvature upon the anisotropy of the turbulence structure, the quantities $2L_{vv}/L_{uu}-1$ and $2L_{ww}/L_{uu}-1$ are plotted *vs.* $\tau-\tau_0$ in figure 7; both quantities vanish in isotropic turbulence. In the straight section, these anisotropies generally took values in the range between -0.3 and -0.4. In the high-shear flows, curvature generally tended to increase the ratio L_{vv}/L_{uu} in cases with negative S and to decrease it in cases with positive S. It had the opposite effect on the ratio L_{ww}/L_{uu}, although less pronounced. In the low-shear flows, the same trends were observed for L_{vv}/L_{uu}, but L_{ww}/L_{uu} seemed to be insensitive to curvature. In any case, remember that Eulerian integral lengthscales,

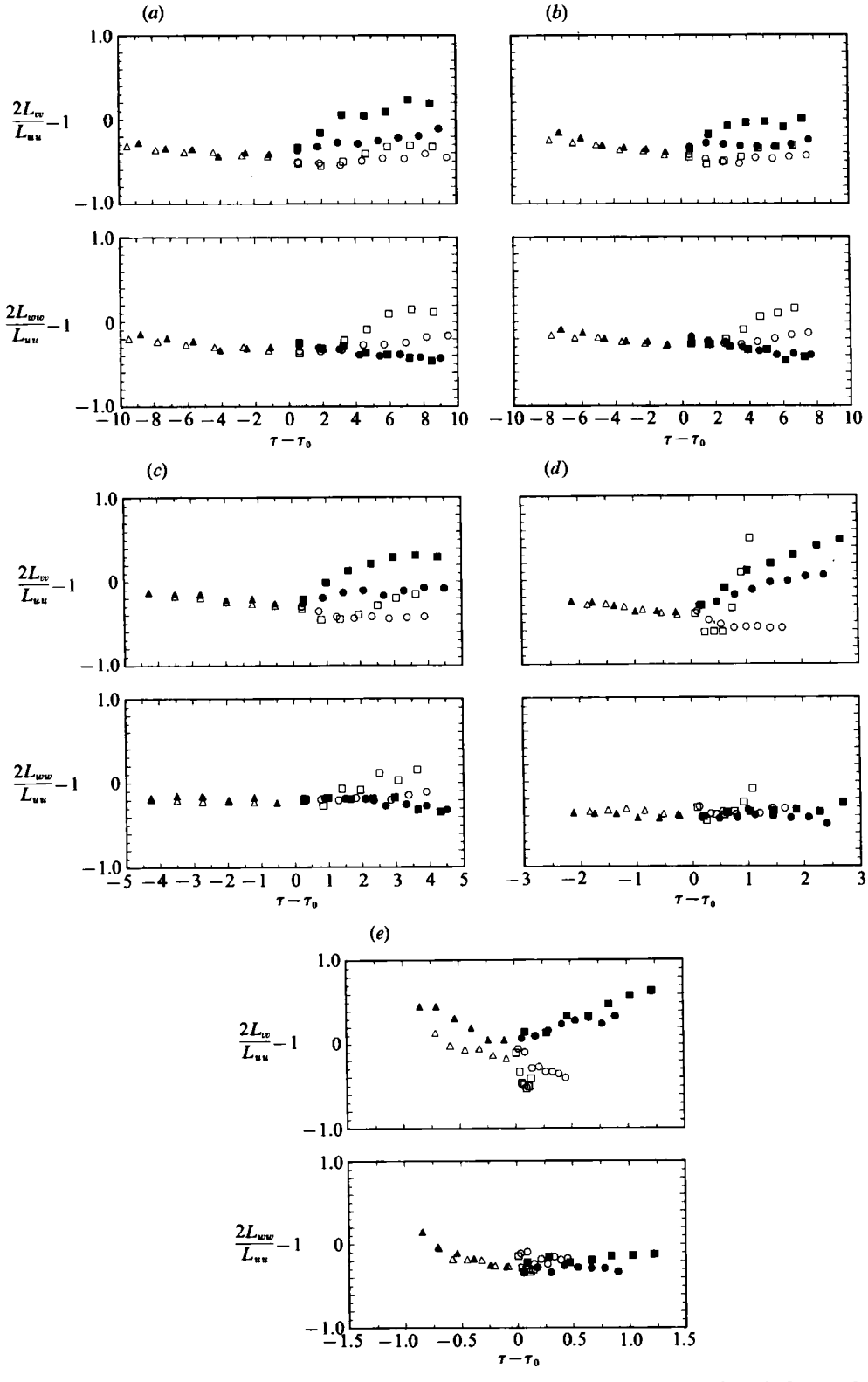

FIGURE 7. Evolution of the anisotropy of integral lengthscales along the wind tunnel centreline. Cases and symbols as in figure 3.

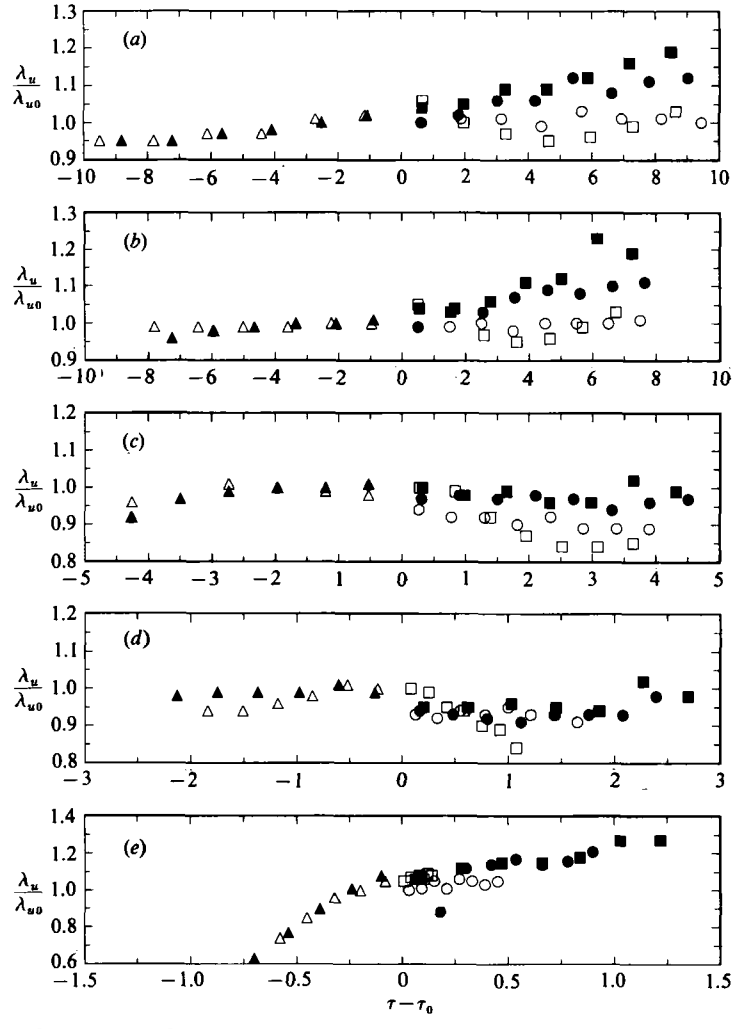

FIGURE 8. Evolution of the streamwise Taylor microscale along the wind tunnel centreline. Cases and symbols as in figure 3.

computed by integrating the corresponding autocorrelation functions to their first zeros, are only crude indicators of the size of turbulent eddies, and that flows with comparable values of such scales could have vastly different structures.

7.6. *Taylor microscales*

In general, in both the straight and the curved sections, the Taylor microscales exhibited streamwise, spanwise and transverse variations that were small compared to the streamwise variations of the kinetic energy and the integral lengthscales. The anisotropies of the Taylor microscales were also relatively small, as evidenced by table 4, showing the ratios λ_v/λ_u and λ_w/λ_u in the straight section. Figure 8 shows that curvature had an effect of slightly increasing λ_u when negative and slightly decreasing it when positive. Curiously, curvature effects on λ_u were more visible in the high-shear than in the low-shear flows.

8. Analysis of the results and discussion

8.1. *On the stability of curved shear flow*

The present experiments include cases for which the energy of turbulence grew and decayed roughly exponentially. Stability analyses of curved shear flows, such as a circular Couette flow, have also predicted exponential growth or decay of the energy of introduced disturbances.

The simplest and most easily applied criterion for instability of curved shear flow is that of Rayleigh (1916), which gives the necessary and sufficient condition for the instability of an arbitrary disturbance of the base motion in inviscid flow as

$$\frac{\partial}{\partial n}[U(n+R_c)]^2 < 0. \tag{40}$$

Equation (40) implies that, if the square of the angular momentum of the base motion decreases outward from the centre of curvature, the flow would be unstable; otherwise the flow would be unconditionally stable.

One might explore the possible application of this criterion to a turbulent flow by considering the mean velocity as the base motion and the velocity fluctuation as a disturbance. Obviously, this analogy is seriously limited by the differences between an inviscid flow and a (highly dissipative) turbulent flow. Nevertheless, one may evaluate the implications of (40) for the present flow, which has a linear mean velocity. In this case, the necessary and sufficient condition for instability on the wind tunnel centreline ($n = 0$) is $S < -1$, with the limiting case corresponding to irrotational motion (a potential vortex). The present experiments suggest that flows for which $S < 0.05$ show growing stresses. Therefore, it appears that Rayleigh's criterion cannot provide, even approximately, the threshold value of S that separates flows with growing turbulent stresses from those with decaying ones.

8.2. *Towards a quantitative description of weak curvature effects*

It has so far been clearly demonstrated that the turbulence structure in the curved sections has a systematic dependence upon the curvature and that the values of dimensionless flow parameters depend monotonically upon the value of S. Among the cases studied, there is a good degree of confidence in the results obtained in the twelve high-shear cases A, B and C. Therefore, it seems worth consolidating these results into a set of semi-empirical, analytical expressions, which could be useful for comparisons with the results of theories and models. The results in the low-shear cases D and E were, generally, consistent with the trends observed in the high-shear cases. Nevertheless, because of the relative immaturity of these flows and the reduced confidence in the accuracy of measurements of S, τ etc., the low-shear results will not be used in the present, quantitative description.

Among the independently measured parameters, the one that appears to be both very sensitive to curvature and measurable with good accuracy is the dimensionless shear stress, K_{uv}. For the high-shear flows at least, K_{uv} had a sign opposite to the sign of S and a magnitude that decreased with increasing S. The high-shear results, collected in figure 9, can be reasonably well represented by the linear, least-squares fit

$$K_{uv} = -0.14(1-3.0S)\,\mathrm{sgn}\,S. \tag{41}$$

Then, the 'production' of turbulent kinetic energy can be represented as

$$P^* = 0.14(1-3.0S)\,(1-S). \tag{42}$$

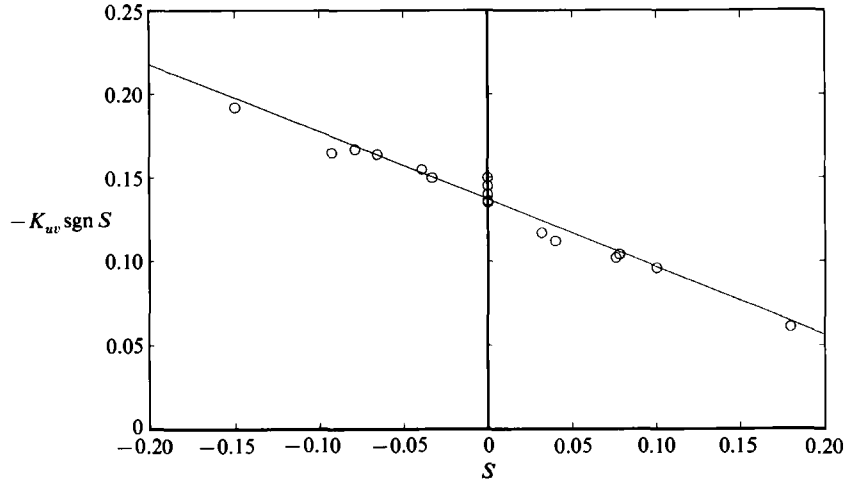

FIGURE 9. The dependence of K_{uv} on S in the high-shear flows. The solid line represents a least-squares fit to the data (equation (41)).

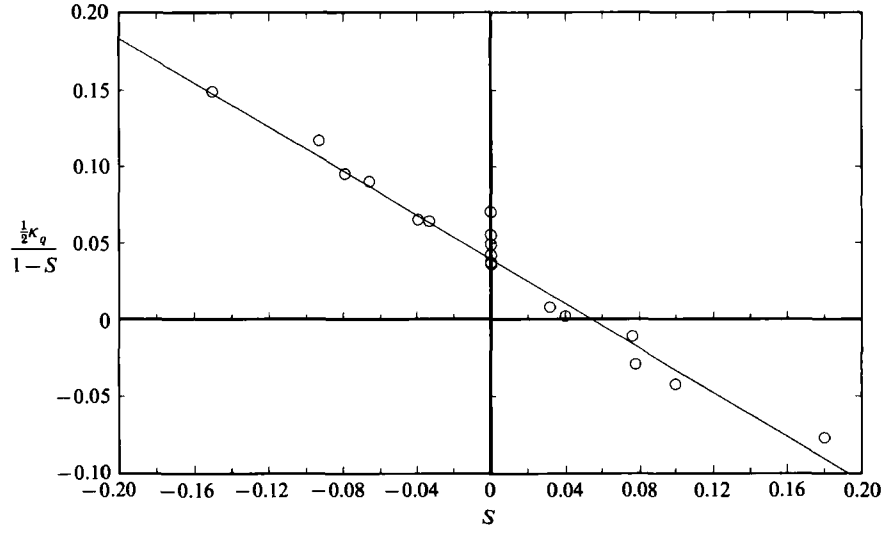

FIGURE 10. The dependence of κ_q on S in the high-shear flows. The solid line represents a least-squares fit to the data (equation (43)).

As mentioned earlier, it seems likely that K_{uv} would reach constant, asymptotic values for very large positive or negative values of S. With this in mind, one can view the linear expression (41) as the tangent, at $S = 0$, of a more complicated function of S (e.g. one that has an error-function-type shape).

A second, independent, empirical relationship between a turbulent parameter and S is further required. The dimensionless 'convection' of kinetic energy, $\frac{1}{2}\kappa_q$, was readily measurable, although subject to errors larger than those pertaining to the measurement of P^*. Measurements of the ratio $\frac{1}{2}\kappa_q/(1-S)$ in the high-shear flows, shown in figure 10, appear to be compatible with the linear relationship

$$\frac{\frac{1}{2}\kappa_q}{1-S} = 0.039(1-18.5S), \tag{43}$$

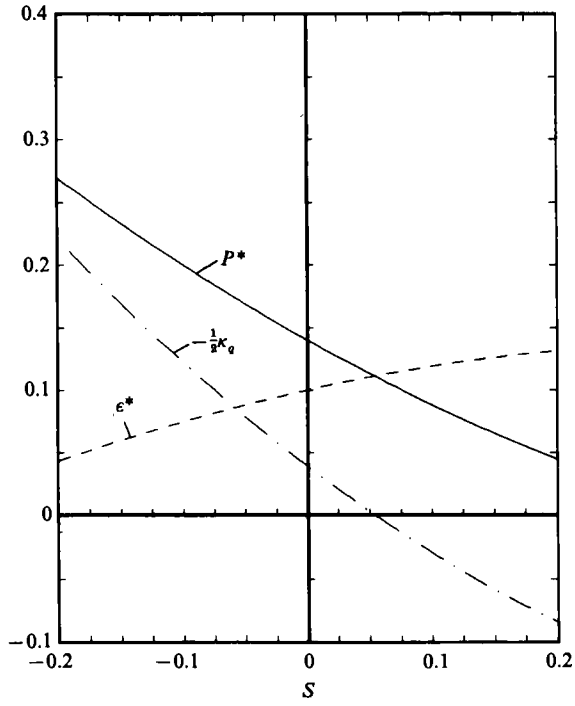

FIGURE 11. Dependence of the production, P^*, convection, κ_q, and dissipation, ϵ^*, of the turbulent kinetic energy upon the parameter S in high-shear flows.

which leads to the following expression for the dimensionless 'dissipation':

$$\epsilon^* = 0.10(1+3.2S)(1-S). \tag{44}$$

The inferred dependences of the dimensionless production, convection and dissipation upon S are illustrated in figure 11. P^* decreased monotonically with increasing S, pointing to a possible sign reversal at sufficiently large, positive S, although this would be outside the range of the present approximation. The ratio ϵ^*/P^* was about 0.7 at $S = 0$ and increased monotonically with increasing S, while the ratio $\frac{1}{2}\kappa_q/P^*$ showed the reverse trend.

The above expressions should describe the measurements fairly well in the range $-0.15 < S < 0.15$ and, with some reservations, possibly in the extended range $-0.25 < S < 0.25$. One must refrain, however, from further extrapolating these expressions, as this could lead to inaccuracies and to possible physical absurdities, such as $\epsilon^* < 0$.

8.3. *Estimates of the pressure–strain rate covariances*

Using the previously derived empirical expressions for K_{uv} and κ_q and the average values $K_{uu} \approx 0.48$, $K_{vv} \approx 0.21$ and $K_{ww} \approx 0.31$, it is possible to compute the small-S dependence of the pressure–strain rate covariances, based on the equations presented in §2.5. These are

$$\phi^*_{uu} = -0.175(1+0.20S-7.6S^2), \tag{45}$$

$$\phi^*_{vv} = 0.084(1+4.5S-18.8S^2), \tag{46}$$

$$\phi^*_{ww} = 0.091(1-3.7S+2.7S^2), \tag{47}$$

$$\phi^*_{uv} = 0.199(1-2.5S-4.2S^2+3.0S^2)\,\mathrm{sgn}\,S \tag{48}$$

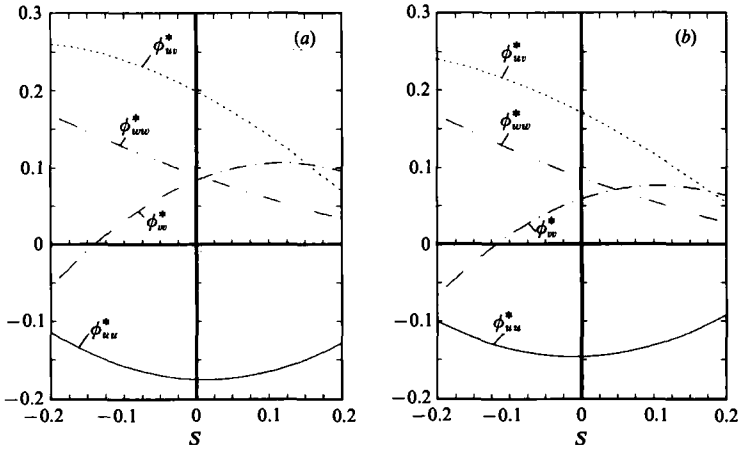

FIGURE 12. Variation of the pressure–strain rate covariances, calculated from the balance of the Reynolds stress equations and based on (*a*) the isotropic and (*b*) an anisotropic model of the dissipation.

for an isotropic dissipation, and

$$\phi^*_{uu} = -0.146(1-0.15S-8.5S^2), \tag{49}$$

$$\phi^*_{vv} = 0.059(1+5.5S-25.6S^2), \tag{50}$$

$$\phi^*_{ww} = 0.087(1-4.0S+3.0S^2), \tag{51}$$

$$\phi^*_{uv} = 0.171(1-2.8S-3.4S^2+2.1S^3)\,\mathrm{sgn}\,S \tag{52}$$

for a dissipation tensor with the same anisotropy as the Reynolds stress tensor. Both sets of expressions are plotted *vs.* S in figure 12. This figure shows that, in general, $\phi^*_{uu} < 0$ and $\phi^*_{ww} > 0$ in the present range, while ϕ^*_{vv} is slightly negative for large, negative S and positive otherwise.

It is generally accepted that, in rectilinear shear flows, the pressure–strain rate covariances provide coupling among the Reynolds stress equations and redistribute the energy from the streamwise energy component to the transverse and spanwise components. A pressure–strain covariance also contributes to the production of shear stress. In addition to these observations, which also apply to curved flows, one may also note the following effects.

When $S > 0$, the correlation between pressure and strain rate fluctuations appeared to diminish and, therefore, to play a less significant role in the kinetic energy partition. In this case, the transverse component received more energy from the streamwise component than the spanwise component did. However, when $S < 0$, the energy transferred from the streamwise component to the spanwise component exceeded that transferred to the transverse component. For the more extreme cases of negative S, all the energy transfer from the streamwise component went to the spanwise component, which also received energy from the transverse component.

For both the isotropic and anisotropic models of dissipation rate, and presumably for any conditions which lie between these extremes, the pressure–strain rate covariances were strong functions of S and played an important role in the determination of the Reynolds stress.

8.4. *Comparison to curved boundary layers*

Rectilinear, uniformly sheared flows are known to have properties comparable to those in the outer regions of two-dimensional, turbulent boundary layers (Tavoularis & Corrsin 1981). It seems worth examining the extent by which curved homogeneous shear flows would be similar to curved inhomogeneous flows, particularly curved boundary layers. Because the curvature parameter, S, varies strongly across a boundary layer, such comparisons can only be qualitative.

The strength of the curvature in boundary layers can be characterized by the ratio δ/R, where δ is the boundary-layer thickness and R is the radius of curvature of the surface. In the present context, $\delta/R = O(S)$, if one makes the crude estimate $A = O(U_\infty/\delta)$. As an example, the mildly curved boundary layers studied by Ramaprian & Shivaprasad (1978*b*) had $\delta/R \approx 0.013$. The same authors have reported that, across most of the boundary layer near a concave wall ($S < 0$), $K_{uv} \approx 0.2$, while, near a convex wall ($S > 0$), $K_{uv} \approx 0.11$. These values are significantly different from the value $K_{uv} \approx 0.16$ measured in a plane boundary layer and compatible with the results obtained in the approximately homogeneous flows.

Curvature effects on lengthscales in homogeneous and boundary-layer flows were also found to be similar. For example, in comparison to the integral lengthscales in a plane boundary layer, the integral lengthscales in a comparable concave boundary layer were found to be larger, while those in a convex boundary layer were found to be smaller. Furthermore, the Taylor microscales in boundary layers were almost unaffected by curvature. Similar observations have been made in the present flows.

8.5. *On the reversal of the shear stress in stabilized flows*

It was noted earlier that, for low-shear flows in the strongly curved section (cases PD and PE), the turbulent shear stress attained the same sign as the mean shear, in sharp contrast with the gradient transport concept as well as with all other observations in nearly homogeneous shear flows with a lower magnitude of S. Rather than being anomalous, these cases further establish the monotonic trend observed in all stabilized flows, namely that curvature tends to produce positive shear stress. The continuing increase of the coefficient K_{uv} in the low-shear PD and PE cases prevents us from establishing a relationship between this coefficient and S, in the large-S range. Since K_{uv} is bounded, such a relationship can be foreseen to approach asymptotically constant values for both very large positive and very large negative S. In these ranges, of course, the effects of mean shear are likely to be small compared to curvature effects, and, therefore, the dimensionless time τ would be irrelevant as an independent variable for the evolution of turbulence structure, because its definition is based on the timescale of the mean shear, $(\mathrm{d}U/\mathrm{d}n)^{-1}$. An alternative dimensionless time, connected with the timescale of the flow curvature, R_c/U_c, would be the turning angle, θ, defined as

$$\theta = \frac{U_c}{R_c}\frac{s}{U_c} = (\tau - \tau_0)\,S. \tag{53}$$

To exploit this possibility, the low-shear measurements of $K_{uv}\,\mathrm{sgn}\,S$ have been plotted *vs.* θ in figure 13. All results essentially collapsed on two monotonic clusters, one decreasing ($S < 0$) and one increasing ($S > 0$). The decreasing cluster appeared to be closer to its asymptote, which was near -0.25, while the increasing cluster demonstrated an essentially linear increase that persisted beyond its last value of

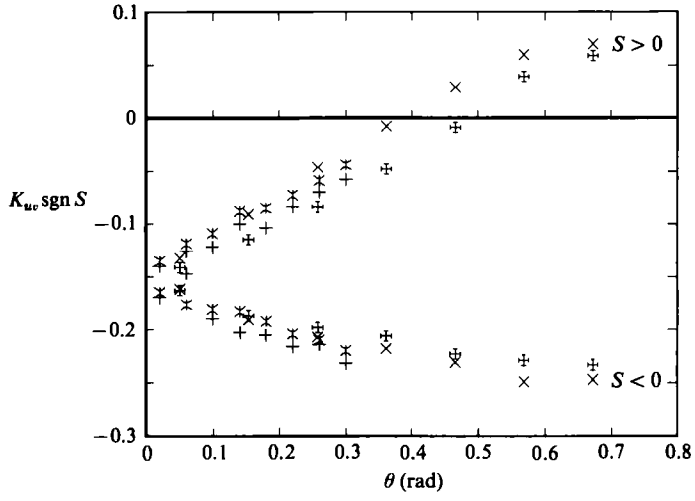

FIGURE 13. Evolution of the dimensionless turbulent shear stress as a function of the turning angle.

about 0.07. If one further speculates that, in the limit of vanishing shear, K_{uv} would become independent of both the magnitude and the sign of S, then one may extrapolate the results in figure 13 to obtain

$$K_{uv} \to 0.25 \quad \text{as} \quad S \to \pm\infty, \tag{54}$$

with the plausible explanation that the negative-S cases approached this asymptote faster (in terms of turning angle) than the positive-S cases did, because their starting values at the end of the straight section were closer to it.

Although sign reversal of shear stress has been observed in strongly inhomogeneous, asymmetric flows (Eskinazi & Erian 1969) and strongly stabilized buoyant flows (Komori *et al.* 1983), this appears to be the first time that this phenomenon has been documented for homogeneous curved shear flows.

9. Conclusions

The present experiments have demonstrated that approximately homogeneous, curved, shear flows can be generated in the laboratory. These flows have displayed two distinct patterns of turbulence development: flows with $S > 0.05$ had decreasing Reynolds stresses and integral lengthscales, while flows with $S < 0.05$ had increasing Reynolds stresses and integral lengthscales. The effect of curvature on the turbulence structure was most clearly displayed by the dimensionless shear stress, K_{uv}, which acquired asymptotically constant values when sufficient development time was available in the facility. These asymptotic values were monotonically decreasing with increasing S. In a qualitative sense, the effects of curvature on nearly homogeneous shear stress were found to be similar to those observed in curved boundary layers.

Financial support for this research was provided by the Natural Sciences and Engineering Research Council of Canada.

REFERENCES

BARLOW, R. S. & JOHNSTON, J. P. 1988*a* Structure of a turbulent boundary layer on a concave surface. *J. Fluid Mech.* **191**, 137–176.

BARLOW, R. S. & JOHNSTON, J. P. 1988*b* Local effects of large-scale eddies on bursting in a concave boundary layer. *J. Fluid Mech.* **191**, 177–195.

BRADSHAW, P. 1973 Effects of Streamline Curvature on Turbulent Flow. *AGARDograph* No. 169. NATO.

CASTRO, I. P. & BRADSHAW, P. 1976 The turbulence structure of a highly curved mixing layer. *J. Fluid Mech.* **73**, 265–304.

CHAMPAGNE, F. H., HARRIS, V. G. & CORRSIN, S. 1970 Experiments on nearly homogeneous turbulent shear flow. *J. Fluid Mech.* **41**, 81–139.

CORRSIN, S. 1963 *Turbulence: Experimental Methods.* Handbuch der Physik, Vol. 8, Part 2 (ed. S. Flügge & C. Truesdell), pp. 523–590. Springer.

DEAN, W. R. 1928 Fluid motion in a curved channel. *Proc. R. Soc. Lond.* A **121**, 402–420.

ESKINAZI, S. & ERIAN, F. F. 1969 Energy reversal in turbulent flows. *Phys. Fluids* **12**, 1988–1998.

ESKINAZI, S. & YEH, H. 1956 Fully developed turbulent flow in a curved channel. *J. Aeronaut. Sci.* **23**, 23–35.

GIBSON, M. M. & VERRIOPOULOS, C. A. 1984 Turbulent boundary layer on a mildly curved convex surface: Part 2, Temperature field measurements. *Exp. Fluids* **2**, 73–80.

GIBSON, M. M., VERRIOPOULOS, C. A. & VLACHOS, N. S. 1984 Turbulent boundary layer on a mildly curved convex surface: Part 1, Mean flow and turbulence measurements. *Exp. Fluids* **2**, 17–24.

GILLIS, J. C. & JOHNSTON, J. P. 1983 Turbulent boundary layer and structure on a convex wall and its redevelopment on a flat wall. *J. Fluid Mech.* **135**, 123–153.

GÖRTLER, H. 1940 Über eine dreidimensionale Instabilität laminarer Grenzschichten an konkaven Wänden. *Nachr. Ges. Göttingen, Math.-Phys.* K1, 2.

HARRIS, V. G., GRAHAM, J. A. H. & CORRSIN, S. 1977 Further experiments in nearly homogeneous turbulent shear flow. *J. Fluid Mech.* **81**, 657–687.

HINZE, J. O. 1975 *Turbulence*, 2nd edn. McGraw Hill.

HOFFMAN, P. H., MUCK, K. C. & BRADSHAW, P. 1985 The effect of concave surface curvature on turbulent boundary layers. *J. Fluid Mech.* **161**, 371–403.

HOLLOWAY, A. G. L. 1989 The effects of curvature on sheared turbulence. Ph.D. dissertation, University of Ottawa.

HUNT, I. A. & JOUBERT, P. N. 1979 Effects of small streamline curvature section turbulent duct flow. *J. Fluid Mech.* **91**, 633–659.

KARNIK, U. & TAVOULARIS, S. 1987 Generation and manipulation of uniform shear with the use of screens. *Exp. Fluids* **5**, 247–254 (referred to herein as KT).

KOMORI, S., UEDA, H., OGINO, F. & MIZUSHINA, T. 1983 Turbulence structure in stably stratified open-channel flow. *J. Fluid Mech.* **130**, 13–26.

KOYAMA, H. S. 1981 Turbulent shear flows behind cylinder and sphere in curved channels. In *Proc. 3rd Symp. Turbulent Shear Flows, Davis, USA*, pp. 4.12–4.16.

MARGOLIS, D. P. & LUMLEY, J. L. 1965 Curved turbulent mixing layer. *Phys. Fluids* **8**, 1775–1785.

MERONEY, R. N. & BRADSHAW, P. 1975 Turbulent boundary layer growth over a longitudinally curved surface. *AIAA J.* **13**, 1448–1453.

MOSER, R. D. & MOIN, P. 1987 The effects of curvature in wall bounded turbulent flows. *J. Fluid Mech.* **175**, 479–510.

MUCK, K. C., HOFFMAN, P. H. & BRADSHAW, P. 1985 The effect on convex surface curvature on turbulent boundary layers. *J. Fluid Mech.* **161**, 347–369.

NAKANO, S., TAKAHASHI, A., SHIZAWA, T. & HONOMI, S. 1981 Effects of stable and unstable free streams on a turbulent flow over a concave surface. In *Proc. 3rd Symp. Turbulent Shear Flows, Davis, USA*, pp. 4.18–4.23.

RAMAPRIAN, B. R. & SHIVAPRASAD, B. G. 1978*a* Turbulence measurements in boundary layers along mildly curved surfaces. *Trans. ASME* I: *J. Fluids Engng* **100**, 37–46.

RAMAPRIAN, B. R. & SHIVAPRASAD, B. G. 1978*b* The structure of turbulent boundary layers along mildly curved surfaces. *J. Fluid Mech.* **85**, 272–303.

RAMAPRIAN, B. R. & SHIVAPRASAD, B. G. 1982 The instantaneous structure of mildly curved turbulent boundary layers. *J. Fluid Mech.* **115**, 39–58.

RAYLEIGH, LORD 1916 On the dynamics of revolving fluids. *Scientific Papers*, Vol. 6, 447–453.

SAVILL, A. M. 1983 The turbulence structure of a highly curved two-dimensional wake. In *Structure of Complex Turbulent Shear Flow, IUTAM Symp., Marseille* (ed. R. Dumas & L. Fulachier). Springer.

SHIZAWA, T. & HONAMI, S. 1985 Experiments on turbulent boundary layers over a concave surface – Response of turbulence to curvature. In *Proc. 5th Symp. Turbulent Shear Flows, Ithaca, USA*, pp. 21.1–21.6.

SMITS, A. J., YOUNG, S. T. P. & BRADSHAW, P. 1979 The effect of short regions of hish surface curvature on turbulent boundary layers. *J. Fluid Mech.* **94**, 209–242.

SO, R. M. C. & MELLOR, G. L. 1973 Experiment on convex curvature effects in turbulent boundary layers. *J. Fluid Mech.* **60**, 43–62.

SO, R. M. C. & MELLOR, G. L. 1975 Experiment on turbulent boundary layers on a concave wall. *Aeronaut. Q.*, February, 25–40.

SYNGE, J. L. 1933 The stability of heterogeneous liquids. *Trans. R. Soc. Canada* **27**, Series 3, Section 3, 1–18.

SYNGE, J. L. 1938 On the stability of a viscous liquid between rotating coaxial cylinders. *Proc. R. Soc. Lond.* **167**, 250–256.

TAVOULARIS, S. 1985 Asymptotic laws for transversely homogeneous turbulent shear flow. *Phys. Fluids* **28**, 999–1001.

TAVOULARIS, S. & CORRSIN, S. 1981 Experiments in a nearly homogeneous shear flow with a uniform mean temperature gradient. Part 1. *J. Fluid Mech.* **104**, 311–347.

TAVOULARIS, S. & KARNIK, U. 1989 Further experiments on the evolution of turbulent stresses and scales in uniformly sheared turbulence. *J. Fluid Mech.* **204**, 457–478 (referred to herein as TK).

TAYLOR, G. I. 1923 Stability of a viscous liquid contained between two rotating cylinders. *Phil. Trans. Roy. Soc. Lond.* A **223**, 289–343.

WYNGAARD, J. C., TENNEKES, H., LUMLEY, J. L. & MARGOLIS, D. P. 1968 Structure of turbulence in a curved mixing layer. *Phys. Fluids* **11**, 1251–1253.